NTNU
Det skapende universitet

Applikasjon av fokusert ionestråle (FIB) og skanning elektronmikroskop (SEM) for karakterisering av vev, celler og biomaterialer.

Ken Roger Ervik

Nanoteknologi
Oppgaven levert: Juni 2011
Hovedveileder: Pawel Tadeusz Sikorski, IFY

Norges teknisk-naturvitenskapelige universitet

Declaration of independent work

I hereby declare that the work in this project has been performed independently and in accordance with the examination regulations of Norwegian University of Science and Technology (NTNU).

_____

Ken Roger Ervik

Abstract

In this study, it is intended to investigate characterization possibilities with a focused ion beam (FIB) combined with a scanning electron microscope (SEM). Aspects of the sample preparation, image acquisition and processing have been discussed. Accomplishments include acquiring 3D data from two structurally very different materials; Structural information of biopolymer alginate hydrogel beads (critical point dried). Of this material image stacks with a resolution of 25 nm (slice thickness) in the z-direction has been acquired. The second material is cells (macrophages from mouse) embedded in an epoxy resin. From this type of sample there has been retrieved image stacks with 30 and 40 nm between each section, where cellular structures and organelles are clearly resolved. Also, a 3D reconstruction of cell tissue is done.

Preface

This master thesis is written under the supervision of Associate Professor Pawel Sikorski at the Department of Physics, Faculty of Natural Sciences and Technology, NTNU, and is a continuation of the project work *"Characterizing alginate beads with Confocal Laser Scanning Microscopy, Scanning Electron Microscopy and Focused Ion Beam"* which I finished December 2010 [1]. Some of the literature studies done in the preceding project is still relevant and will appear in the Theory section.

In this study I intend to demonstrate FIB-SEM as a characterization technique with high quantitative efficiency and gain initial competence in requirements for the samples, data collection and data analysis. No experience of characterizing biological samples with a FIB-SEM exists on a national basis, and is also scarce world wide. A lot of time has been spent in the NTNU NanoLab cleanroom operating and learning how to handle my samples with the FIB. It has truly been exciting and satisfying to be able to explore a new technique of investigating biological specimens and hopefully contribute to pushing the frontier of characterization further.

A successful collaboration with the group of Professor Kåre Tvedt and Researcher Øyvind Halaas at The Medical Faculty at NTNU has been most helpful in providing customary made samples. Their interest in the project have kept pushing my research forward. The work done here will hopefully increase interest of FIB related to the field of bionanotechnology at NTNU NanoLab as a powerful characterization tool in the research community at NTNU.

Acknowledgements

First of all, I would like to thank my supervisor Associate Professor Pawel Sikorski for all his support. His enthusiasm has been imperative for my own motivation and progression of my work. Not only have I gotten to know him in an educational setting, but also enjoy conversing with him about everyday life. It has been a pleasure working with him. I must also show my gratitude to Post doc. Minli Xie for producing alginate beads for me and being supportive.

I acknowledge Professor Kåre Tvedt and Researcher Øyvind Halaas for their interest in my project. They have shown great enthusiasm to my work, which has motivated me and kept me patient. They have provided support when it comes to the medical aspect of the project for which I am grateful.

I would also like to thank Engineer Nan E. Tostrup Skogaker for taking the time to

prepare samples for me. I have recognized her talent of sample preparation, and greatly appreciate her cooperation.

I must also show my appreciation of the NanoLab staff, Chief Engineer Søren Heinze, Staff Engineer Ida Noddeland and Staff Engineer Espen Rogstad for their support and cooperative attitude regarding technical support at the NTNU NanoLab. And, also, for keeping the NanoLab a safe environment to work in.

Last but not least, I must thank my friends and fellow students for giving me an experience of a lifetime. It has truly been inspiring to work together over five years, and I feel lucky to be a part of such a strong companionship. I have met some of my best friends here at NTNU and hopefully we will continue to stay in touch as we now part ways.

Contents

1 Introduction

In the field of characterization of biological materials, tools like Confocal Laser Scanning Microscopy (CLSM) and Transmission Electron Microscopy (TEM) are traditionally used [2, 3]. Confocal microscopy is an easy-to-use and cell-friendly approach and lets one photochemically stain and get excellent contrast between different components of a cell. Another strength of the CLSM is its ability to acquire 3D data from the samples [4]. However, optical imaging systems like CLSM, have a limited maximum resolution of approximately 200 nm due to the diffraction limit, which is too large when the research requires to study *e.g.* cell organelles with features smaller than 100 nm [5].

When high resolution is needed, TEM is the tool of choice which provides excellent resolution of 2-3 Å for biological samples [6, 7]. A drawback with TEM is the high requirement of the sample. A good TEM-sample takes time to prepare and is required to be sub-100 nm of thickness, which is a challenge as there is a high risk of producing artefacts in the sample (*e.g.* from ultramicrotoming, which can lead to deformation)[8]. Also, the demand of 3D information at high resolution is imminent, and is increasingly needed to answer medical questions. It is possible to acquire image stacks with conventional serial-section TEM, however, it is a very technically demanding and costly task. This is due to that each slice needs to be prepared and imaged separately, and that there is a great risk of introducing artefacts in each section. This makes it very difficult to obtain large numbers of correlative images [8]. Additionally, there is also a limitation of how large (area) the samples sections can be. The larger the section area is, the greater the probability is of getting an non-uniform cut section, thus limiting the volume of interest that can be studied in three dimensions.

Scanning Electron Microscope is also often used to study biological samples [9, 10]. Since the sample needs to be inserted into a vacuum chamber in order to be imaged with the electron beam, there can not be any liquids present in the specimen [11]. Due to this requirement, samples like cells and tissue will loose their structural shape and strength when the liquid is removed during the sample preparation. Loss of mechanical strength requires using a low electron beam voltage to limit destruction of the sample [12]. Also, the electron signal from biological material is from low-energy electrons, which contributes to a weak contrast in biological specimens [13]. For these reasons, biological sample preparations include fixation to maintain the shape as close to its natural state as possible, and staining, using an electron-dense material, like OsO_4 (chemically cross-linking to lipids in *e.g* membranes), to increase the contrast at low electron beam voltages [14].

Focused Ion Beam (FIB) is a comprehensive characterization tool which consist of an ion beam capable of cutting a sample with nanometer precision. Combined with a SEM, it allows one to monitor and image what work is being done with the ion beam [15]. In a biotechnological context this approach is relatively new. The main intention of the FIB system was to improve the resolution and speed of the lithographic technique for the semiconductor industry, when it was developed in the 1960s and commercialized in the 1980s [16, 15]. As of today, different approaches have been tried to use the FIB-SEM for imaging cells [17, 18, 19]. A promising method includes imaging a block face with high-energy electrons after sections are sequentially removed with the ion-beam. In this way it is possible to retrieve high resolution 3D data from the sample and at the same time avoid loss and deformation of sections as in TEM. Additionally, FIB-SEM is capable of milling sections and acquiring images automatically, making the image acquisition process less laboursome. This approach makes it possible to retrieve 3D data within hours, opposed to retrieving 3D data from TEM where it can take weeks and maybe months. Although the FIB-SEM does not provide the same resolution as TEM (typically 0.2-0.3 nm), it still is able to resolve ultrastructural features. Since the application of FIB in biotechnology is relatively new, there is a vast need for developing sample preparation and the ion-milling procedures. There is now more attention towards using FIB on biological materials as more and more papers are published where this technique is used [20, 21, 22].

1.1   Current applications of FIB-SEM to biological samples.

FIB has been used in few recent, high impact publications, where the description of the sample architecture in 3D with nm-resolution was essential for answering a medical question.

In 2009, Schroeder-Reiter *et al.* studied the 3D architecture of chromosomes by milling away slices of the sample so that the a cross-section is exposed. By taking SEM images of each cross-section of the chromosome, they acquired an image stack image representing the milled volume. The slice thickness was in the range of 7-20 nm. This allowed for a high resolution three-dimensional reconstruction as seen in figure 1. They could for the first time show that the chromosome interior is characterized by a network of interconnected cavities with openings to the chromosome surface. The DNA in the chromosome interior could be directly analysed in a three dimensional context when staining with a DNA-specific platinorganic compound [20].
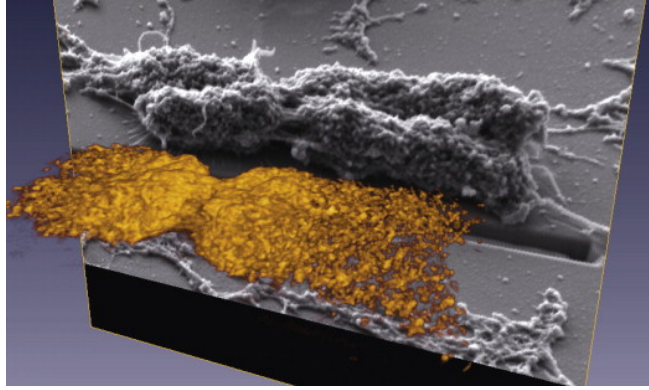
Figure 1: *To the left:* Volume-rendering 3D reconstruction from a series of 198 sections of BSE signals from FIB-SEM sections of a barley metaphase chromosome and corresponding oblique view SE image of whole chromosome (greyscale)(Schroeder-Reiter *et al.*, 2009 [20]).

Knott *et al.* (2008) embedded brain tissue in epoxy resin (using modified transmission electron microscopy sample preparation protocol) and serially sectioned the sample with the ion beam, together with collecting SEM images of the sectioned sample face. In figure 2 is an back-scattered electron image (BSE) of brain tissue [21]. Knott *et al.* managed to retrieve image stacks with excellent contrast, which is an important requirement when the volume is to be reconstructed in three dimensions. In this manner, it was possible to follow the axons and dendrites in a volume of 286 μm^3 and identify their synaptic connections. Visualizing the complete wiring and connections within neural circuits is a realistic challenge with today's EM technology [21]. In the future, this approach can allow to collect images on a large scale through volumes of nervous tissue that may contain complete neural circuits.

Felts *et al.* (2010) studied how the connection between an HIV infection, CD4$^+$ T cells and antigen-presenting cells (macrophages and dendritic cells) greatly enhance the efficiency of the infection [22]. Using FIB-SEM they where able to analyse the spatial architecture of cell-cell contacts and distribution of HIV virions at virological synapses. In figure 3 a 3D reconstruction shows how dendritic cells envelope T cells, thought to form a shielded region for formation of virological synapses. Identifying this scenario has helped scientists understand more of the mechanisms of the HIV infection and

Figure 2: Electron microscopy image of brain tissue sample sliced with FIB (Knott *et al.* [21])

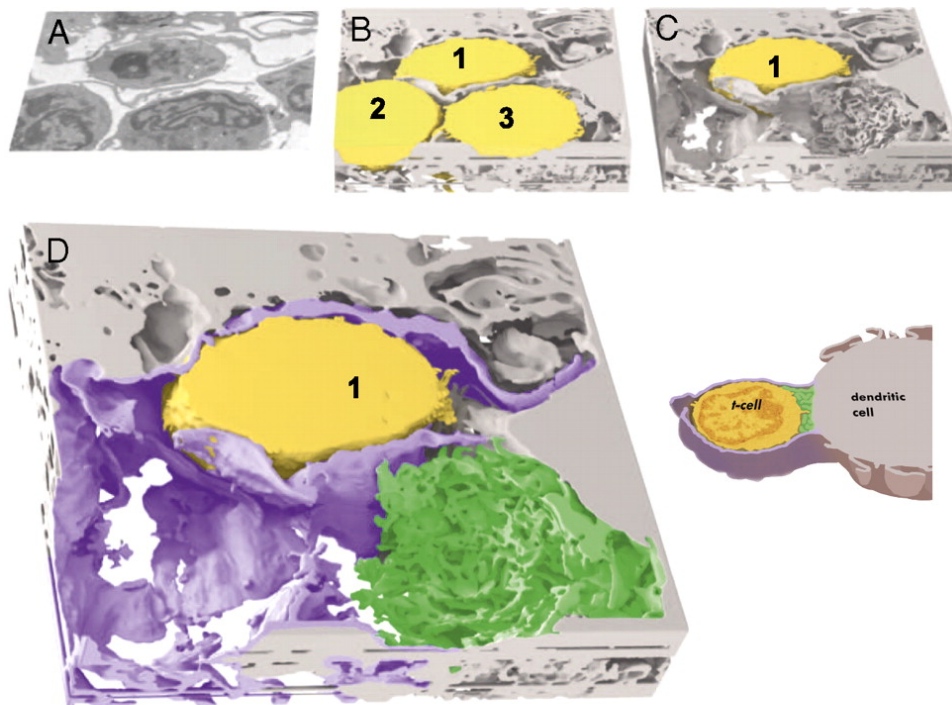gained vital information in the pursue of finding an optimal treatment.

Figure 3: 3D contacts between a dendritic cell and T cell at the synapse visualized with FIB-SEM imaging. (AC) Envelopment of the T cell by sheet-like membrane protrusions from the dendritic cell. The T-cells (numbered 1, 2, and 3) are coloured yellow, and the dendritic cell is shown in light gray. Single-slice (A) and 3D-volume slabs before (B) and after (C) computational removal of the T cells labelled 2 and 3 from the imaged volume are shown. (D) Expanded view of C distinguishing the extensive membrane sheet encasement (purple) and the localized filopodial interdigitations (green) at the region of cell-cell contact emanating from the dendritic cell. A schematic version of the contact is shown to the right [22].

2 Theory

The following section will give support and background for further discussion of the work that has been conducted. Here the main aspects of FIB-SEM is presented.

2.1 Limitation of optical microscopy

CLSM is a conventional microscopy technique in the field of biotechnology [23, 24]. Its main advantages is its ability to eliminate out-of-focus light, only detecting light that originates from the focal plane. A pinhole placed in front of the detector allowing only photons from the illuminated focused spot to pass through, and excluding the photons originating above and below the focal plane. Combined with the possibility to move the focal plane in the z-direction through *e.g.* a cell, gives good results when collecting an image stack (also referred to as a z-stack). The optical sections in the image stack data can be used to reconstruct the cell in three dimensions [25].

However, the resolution of optical imaging systems are fundamentally limited by the diffraction limit given by,

$$d = \frac{0.61\lambda}{NA} \tag{1}$$

where λ is the wavelength and NA is the numerical aperture (typical value of NA=1.4 in modern optics). With light within the visible range (400 - 700 nm) eq. 1 states that the smallest feature that can be resolved is $\sim$ 200 nm [5]. This is large compared to the subunits of a cell, such as organelle features *e.g.* the cristea (internal compartments of mitochondria) which are $\sim$ 40 nm across, or the distance between the inner and outer membranes of a cells nuclei which is separated by 10-50 nm.

2.2 Scanning Electron Microscope (SEM)

The microscope column of the SEM consists mainly of an electron gun, condenser lenses (electromagnetic lenses), scanning coils, probe lenses and a Through-Lens detector, as seen in figure 7. In the vacuum chamber there is a specimen stage and various detector systems, like a Everhart-Thornley detector. When using an electron beam as a probe, incident electrons will interact with the atoms and other electrons at the top surface by scattering. If the scattering energy is high enough to overcome the energy needed for the electrons to escape from the sample and into a vacuum, these electrons can be detected and processed into an image. When looking at surfaces in SEM, there are mainly two

types of electron signals that are detected; secondary electrons (SE) and backscattered electrons (BSE).

2.2.1 Electron signal

The electrons will image the sample with a resolution limited by the spot size of the probe on the sample surface. The spot size is dependant on the wavelength of the electron beam and the instruments ability to focus the beam. The higher the acceleration voltage, the better the beam is focused [26]. The SEM uses electromagnetic lenses to focus the beam to the smallest spot size as possible. However, another element that limits the resolution is the interaction volume, which is the volume where the signal is generated from, as seen to the right in figure 4. The size of the interaction volume is also dependant on the acceleration voltage of the electron beam and on the atomic number of the material in the sample, as the left image in figure 4 shows. The interaction volume is larger than the distance between atoms, which means that the resolution is not high enough to observe individual atoms. This is, however, possible in scanning transmission electron microscopy (STEM), where the samples need to be thin sections (sub 100 nm) [11]. Here the limitation of resolution due to large interaction volume is not an issue. Since the sample is too thin for an appreciatively interaction volume to occur, the resolution will ultimately be limited by the spot size.
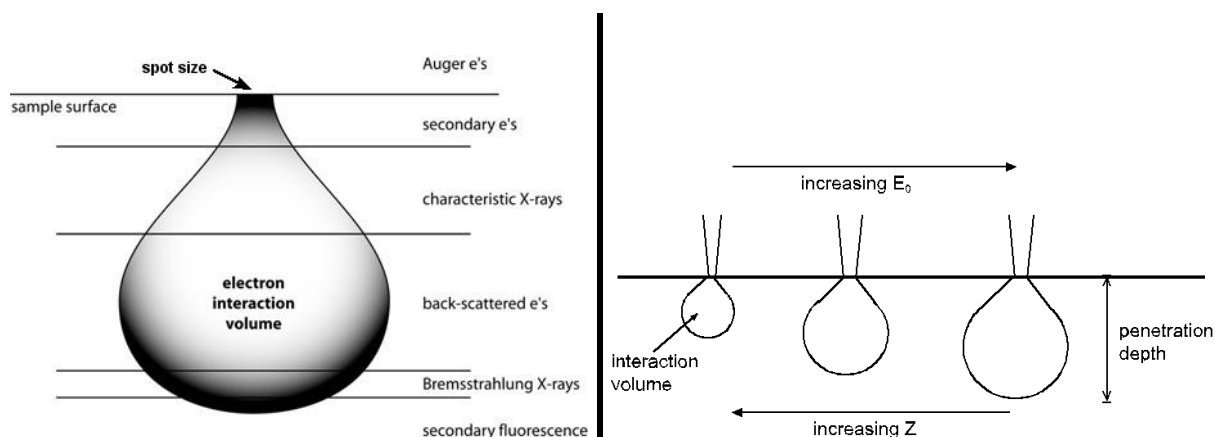

Figure 4: *Left:* Illustration of the interaction volume when the electron beam hits the sample surface.[a] *Right:* Illustration of how the interaction volume changes in size when the energy of the electron beam, E_0, and the atomic number, Z, changes.[b]

The incident electrons (primary beam electrons) will either scatter back with almost no energy loss, or transfer energy to other electrons within the interaction volume. When

---

[a] http://serc.carleton.edu/research_education/geochemsheets/electroninteractions.html
[b] http://laser.phys.ualberta.ca/ egerton/SEM/sem.htm

energy is transferred, some of the electrons can escape as SE. This is called an inelastic collision and the electrons are of low energy, thus only able to emit from near the top surface in the range of 5-50 nm [12, 11]. The shallow depth of origin, make the SEs very sensitive to the topography of the surface. The secondary electrons can be separated into two kinds; Secondary electrons that are generated from the electrons in the incident primary beam, SE_1, and SEs that are generated by BSE, SE_2 [27], as seen in figure 5. There is also a third contribution, SE_3, which will originate from the pole piece of the electron column and basically generate noise in the signal (see figure 5).

BSEs are a result of elastic scattering, where primary electrons from the electron beam are scattered back with almost no energy loss. The electrons re-emerge from within a deeper and larger interaction volume than SE. Due to this larger volume, the resolution in BSE images are poorer than SE images. However, elements of higher atomic number gives a stronger signal than elements with lower atomic number. This is because heavy elements backscatter electrons more strongly and will appear brighter in the image [12]. However, a comparison of the ratio of SE to BSE shows that there is a significantly higher proportion of BSE generated compared to SE as the atomic number increases [14, 11]. Therefore, BSEs are used to resolve local atomic variations on the sample surface, referred to as Z-contrast.

Figure 5: Schematic illustration of how different kinds of secondary electron, SE_1, SE_2 and SE_3, are generated.[c]

Figure 6 shows a spectrum of the electron count versus the electron energy, indicating that the probability of emitting SE is high at low energies, while the BSE have their highest count at just below the energy of the electron acceleration voltage, E_0 [11].
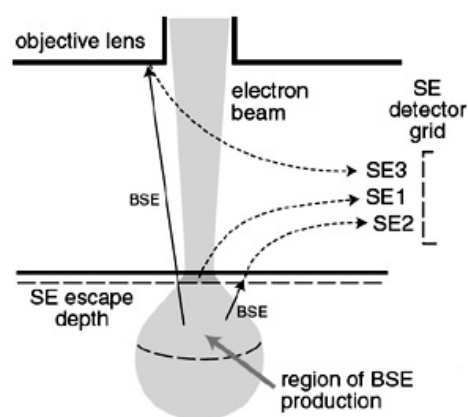

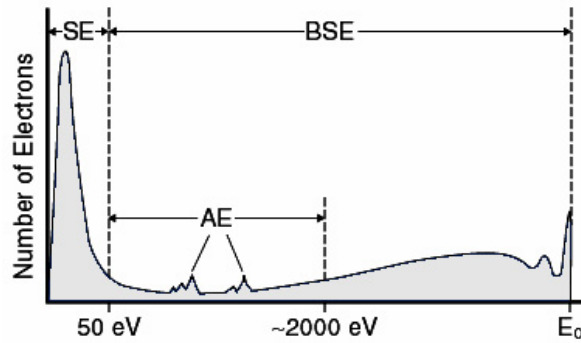[c]http://www4.nau.edu/microanalysis/Microprobe-SEM/Signals.html

Figure 6: Spectrum of the electron count vs electron acceleration voltage. The secondary electrons (SE) display a large low-energy peak, while the backscattered electrons (BSE) mainly originate from high-energy peaks.[d]

The image is collected by scanning the electron probe across the surface of the specimen in a x-y raster [11]. There are two electron detectors; a conventional Everhart-Thornley Detector (ETD) which is placed inside the vacuum chamber and usually used to detect secondary electrons, and a Through-Lens Detector (TLD) placed in the microscope column intended to collect high-energy electrons such as back-scattered electrons and SE_1 (see figure 7). The TLD acquires a high magnetic field which is projected onto the sample surface in order to collect the electrons at a high efficiency. The magnetic field traps the high-energy electrons and spirals them up the column (Lorentz effect) and through the lens pole piece, where they are detected [12].

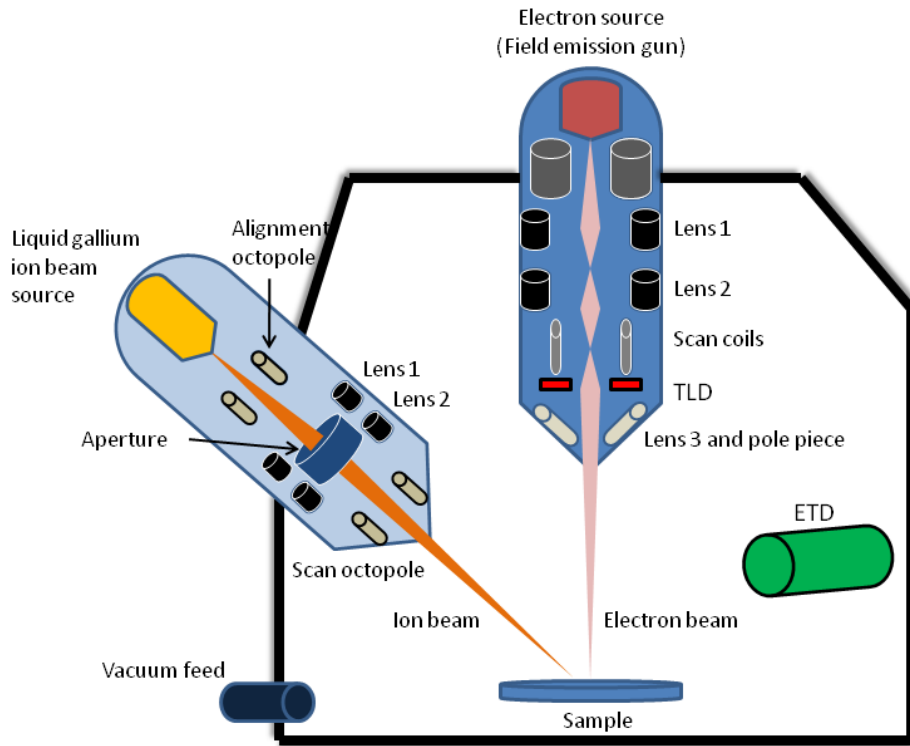
[d]http://www4.nau.edu/microanalysis/Microprobe-SEM/Signals.html

Figure 7: A schematic representation of a Focused ion beam combined with a Scanning electron microscope (Helios NanoLab ^{TM} Dualbeam^{TM}) and its main components. Both instruments share the same vacuum chamber and let the beams operate on the sample simultaneously. The Everhart-Thornley detector (ETD) is placed inside the chamber for mainly detection of low-energy secondary electrons (SE), while the Through-Lens detector (TLD) is placed inside the electron microscope column to detect high-angle, high-energy electrons such as backscattered electrons (BSE) and SE_1.

The most pronounced contrast effect for SE images, comes from the surface topography features. Local curvatures give rise to a difference in the probability for the electrons to escape; surface features with a positive radius will increase the probability for an electron to reach the detector, while a surface feature with a negative radius will decrease the probability [11]. At curvature with positive radius, like sharp edges, an 'edge effect' can be observed, as illustrated in figure 8. Another factor that affects the SE emission is the work function of the surface. The work function is the energy barrier needed to be overcome, by an electron at the Fermi level[e] in the material, in order to be emitted into vacuum [11]. The work function is dependant on material composition, crystal

[e]A measure of the energy of the least tightly held electrons within a solid [28].

structure and surface adsorptions. The latter is a common contamination in SEM as a carbonaceous layer will build up on the sample during electron bombardment. This is due to residual hydrocarbon gases in SEMs equipped with oil-pumped vacuum systems and polymer vacuum seals [12]. This layer can in some cases completely suppress SE contrast if there is no topography.
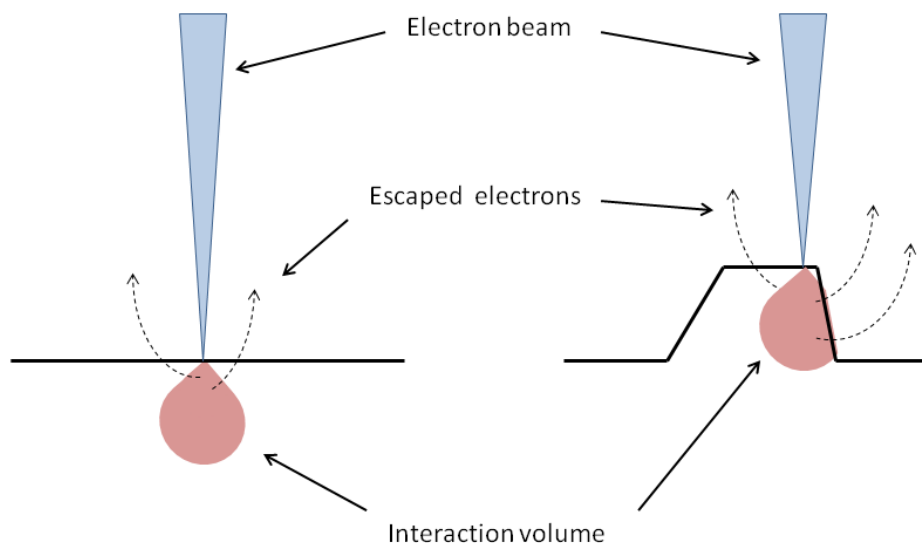

Figure 8: An illustration of the edge effect. When there is a local positive curvature at the surface, there is an increase in probability of electrons escaping giving a brighter signal from the edges of a topographic feature. This is called 'the edge effect'.

As mentioned before, topography contrast relies on SE, while compositional contrast relies on BSE and the atomic number. But it has been reported that compositional contrast can also be observed with SE [29, 30]. Figure 9 shows the relationship between the emitted SE yield, δ, the emitted BSE yield, η, and the atomic number, Z. From the graph there is an increase of the SE yield with Z, but flattens out early as Z becomes higher, which would indicate that the difference in Z is too insignificant to give a clear difference in contrast. However, if the Z number difference is high enough, image contrast can be seen [31]. This means that for a surface that is completely flat, topographic contrast will be ignored, while compositional contrast can be seen given that the difference in atomic number is high enough.
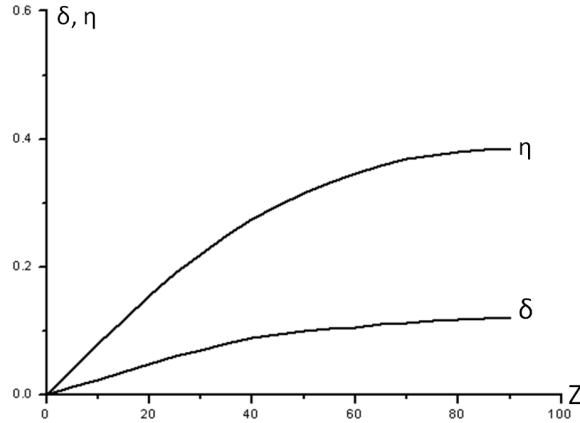
Figure 9: The relationship between the yield of the emitted secondary electrons, δ, the emitted yield of backscattered electrons, η, and the atomic number, Z [31].

2.2.2 Charging

When imaging with an electron beam, a part of the electrons will remain in the specimen as the primary beam electrons loose all their energy and are captured by the specimen. If the specimen is conducting, like a metal, the excess of electrons flow to the ground assuming there is a sufficient ground connection exists. However, if the specimen is insulating, like biological samples, the charge from the trapped electrons will accumulate as the flow of electrons to the ground is too slow. The sample will be in a continuously changing state of surface potential because of charge building up and discharging [12].

The ETD is very sensitive to the electric field lines that surrounds the specimen [12]. When the surface potential changes due to charging, it disrupts the field lines and the collection of SE can be considerably altered. This is manifested in images as bright areas and/or dark areas as the areas are negatively or positively charged relative to the ETD. The problem occurs when the contrast, due to surface potential, overwhelms the contrast from the features of the sample. However, charging does not appear in BSE images in the same amount as SE images, as the surface potential does not alter the trajectories of the high-energy BSE [12]. This means the the charging effects are heavily reduced when collecting BSE, if not entirely.

It must also be mentioned that charging could cause unwanted deflection of an interacting ion beam. This would reduce the positional accuracy of focused ion beam milling (milling will be discussed in section 2.3) [15].

2.3   Focused Ion Beam

Today focused ion beam systems facilitates an increasingly number of research institutes and universities where they function as a characterization tool applicable to the micro- and nanoscale. The FIB-SEM system contains an ion beam primarily for machining, and an electron beam for imaging. The FIB uses a gallium liquid-metal source where the gallium is in contact with a heated tungsten needle. The gallium (melting point 27 ^{o}C) wets the needle, and applying an electric field to it ($\sim 10^8$ volts per cm) will cause ionization and field emission of Ga^+ [15].

In the FIB column there is no *electromagnetic* focusing like in a SEM. An electromagnetic lens in a SEM consists of a coil of copper wire in the iron pole pieces. A current through the coils creates a magnetic field in the bore of the pole pieces, as seen in figure 10. The strength of the magnetic field will be determined by the number of windings of the copper coil and current passing through. When electrons pass through the magnetic field perpendicular to the field lines, the lens is able to control the trajectory of the electron and thus focus an electron beam [12].

Because of the larger mass and energy of ions, *electrostatic* lenses must be used. The reason for this is that a force acting on a charged particle in the FIB is due to an electric field E, $F = qE$, and is independent of the particles velocity, whereas the force exerted by a magnetic field $\mathbf{B}$, $\mathbf{F} = q\mathbf{v} \times \mathbf{B}$, depends directly on the velocity. The acceleration of a particle from a potential difference ΔV is inversely proportional to the particle's mass. It is therefore needed a larger potential difference to give the same velocity gain to an ion compared to an electron. In other words, since the ions have a larger mass than electrons, more force needs to be generated in the lens in order to focus the beam. Electromagnetic optics

Figure 10: An illustration of a electromagnetic lens consisting of a copper coil (green circles) inside an iron bore. When current is passed through the coil, a magnetic field is created (symbolized by red lines). The trajectory of electrons (blue lines) that pass through can be thus be controlled and focused.[f]

would need to be impractically large to provide enough focusing power for the ion beam. However, electrostatic lenses can be of much smaller sizes and produce the required force
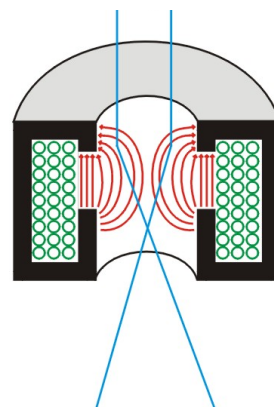
---

[f]http://www.microscopy.ethz.ch/lens.htm

on the ions [15]. As seen in figure 11, an electrostatic lens consists of cylinders with an applied voltage to them. The gap between the cylinders give rise to an electric field and will act as lenses for charged particles that pass through the cylinders. The voltage applied to the cylinders will determine the focusing power, hence the charged particles can be deflected in a controlled manner and focused into a beam. The ion probe is positioned and scanned using quadropoles and octopoles [11].
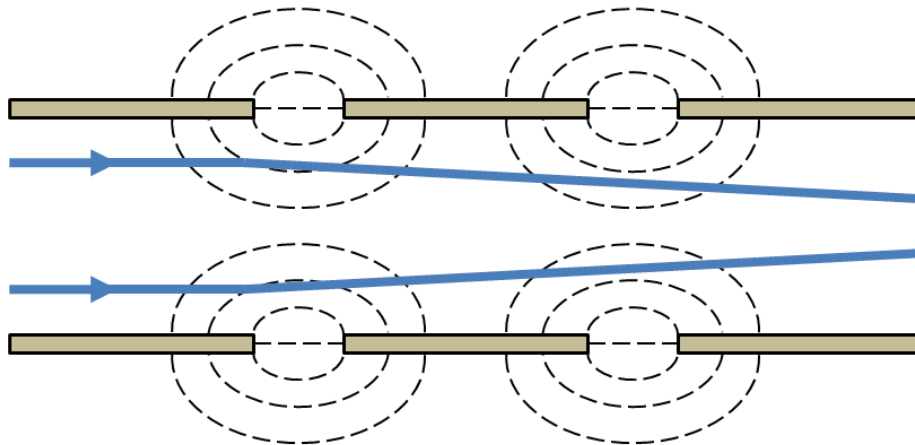

Figure 11: A schematic representation of a cross section of an electrostatic lens consisting of several charged cylinders. The gaps between each cylinder (each having different voltages) creates an electric field (symbolized by the dashed lines). The electric field acts as lenses as they deflect the charged particles passing through and can focus them into a beam.[g]

When using the gallium ion beam, the collision between the ions and atoms in the material is either elastic or inelastic. Elastic collisions occurs when ions collide with the nuclei of the target atoms, and will disturb them from their aligned positions and excavate surface atoms. In other words, the ion beam transfers momentum to the atoms on the surface of the sample which will dissociate from the surface. This dissociation effect of the sample is often termed as *sputtering* or *milling*. The ion beam is capable of removing atoms in such a sputtering effect in a precise and controlled manner. Inelastic collisions result in transfer of energies to the target, leading to a generation of detectable signals like SE, Auger electrons, photons and so forth [15].

Comparing the electron beam and the gallium ion beam in regards to the interaction and imaging of the sample, clearly the gallium ions have have a much more violent encounter with the sample due to the fact that ions have considerably more size and mass, as seen in table 1 [15].

---

[g]http://www4.nau.edu/microanalysis/Microprobe-SEM/Instrumentation.html

	Ga$^+$	Electrons
Particle size	0.2 nm	0.00001 nm
Mass	1.25 x 10^{-25} kg	9.11 x 10^{-31} kg
Velocity at 2 kV	2.8 x 10^5 m/s	1.0 x 10^8 m/s
Momentum at 2 kV	8.8 x 10^{-21} kg m/s	2.4 x 10^{-23} kg m/s
Beam current	pA to nA	pA to μm
Penetration depth polymer at 2 kV	12 nm	100 nm
Penetration depth iron 2 kV	4 nm	25 nm

Table 1: A comparison of different parameters and properties of FIB gallium ions and SEM electrons [15].

2.4   Image processing - Fourier transform

An important tool in image processing is the use of Fourier Transform (FT) to do series expansions of an image function over the image domain (in this case in 2D) into the Fourier domain, also referred to as the frequency domain, displayed as an energy spectrum. The frequency domain is processed before it is transformed back to the spatial domain image, displayed in pixels. In this way it is possible to analyse, filter, reconstruct and compress images.

The image function, $f(a,b)$, with size N×N is decomposed into series of complex expanded functions using the FT,

$$F(k,l) = \sum_{i=0}^{N-1} \sum_{j=0}^{N-1} f(i,j) e^{-i2\pi(\frac{ki}{N} + \frac{kj}{N})} \tag{2}$$

where the exponential term is the basis functions corresponding to each point $F(k,l)$ in the Fourier space. In equation 2 each value in $F(k,l)$ will be acquired by multiplying the image function with the corresponding base function and summing the result , so each point in the Fourier image represents a particular frequency in the image function [32, 33].

When the Fourier Transform image domain needs to be transformed back to the spatial image, the inverse transform is used,

$$f(a,b) = \frac{1}{N^2} \sum_{k=0}^{N-1} \sum_{k=0}^{N-1} F(k,l) e^{i2\pi(\frac{ka}{N} + \frac{kb}{N})} \tag{3}$$

The Fourier Transform produces an output image that contains a complex number value, which can be viewed with either the real (magnitude) or the imaginary (phase)

part. The magnitude contains most of the information of geometric structures in the image and is therefore often displayed. In other words, the magnitude tells how much of a certain frequency is present. The phase tells where this frequency component is in the image. However, when the Fourier image is to be transformed back to the spatial domain (using eq. 3) both the magnitude and phase must be conserved [33, 34, 35]. A simple example of a FT image process is given in figure 12. This figure illustrates how noise (vertical lines) are removed from a picture. The vertical lines transforms into two distinct dots lying horizontally at the center of the Fourier image. By filtering away these dots and transforming back to the spatial domain, the vertical lines are gone. Such vertical stripes seen here are similar to what is seen in SEM images of a cross-section after milling with the ion beam, as seen in figure 42.
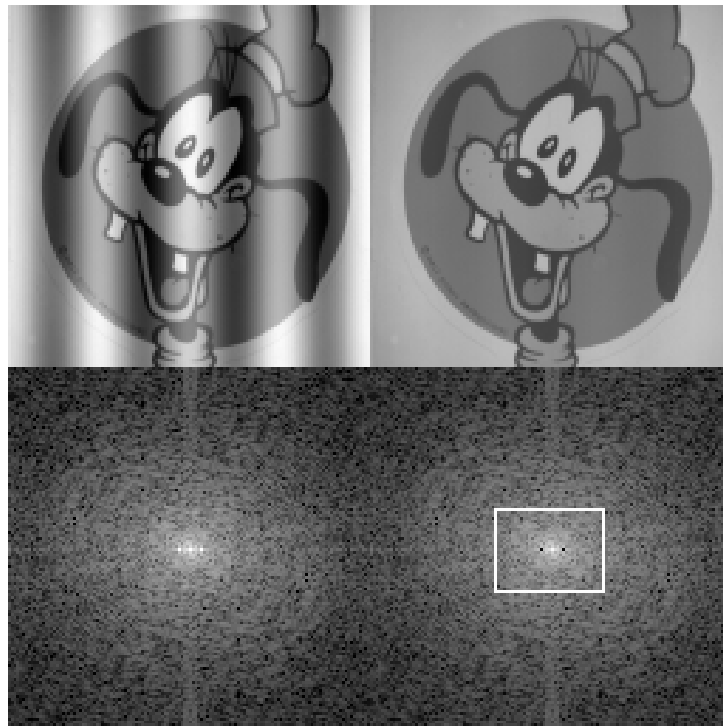

Figure 12: The upper left image shows a picture of Goofy with superimposed noise, in this case, a cosine pattern seen as vertical stripes. The image directly below (lower left) is the Fourier Transform of that image. The two bright distinct dots on each side of the center represent the vertical stripes. In the lower right image these dots have been removed (inside the white box). The upper right image of goofy is the inverse transform of processed image below, where the vertical lines are gone.[h]

---

[h]http://www.cs.unm.edu/ brayer/vision/fourier.html

3 Materials and Methods

3.1 Sample preparation protocols

3.1.1 Preparation protocol for Ca-mineralized beads

The production of beads was done by Post. doc. Minli Xie and done according to Xie *et al.* [36]; Ca-mineralized alginate gel beads (seen in figure 14) were made by dripping a Na-alginate solution into a calcium containing solution using an electrostatic bead generator (see Figure 13). The beads were also critical point dried with a EMITECH K850 Critical Point Drier. The beads where attached to a sample stub with carbon tape, and then sputter coated with a 20 nm thick layer of Pt/Pd (80:20) with a Cressington 208 HR B Sputter Coater. Coating the beads with a metal layer reduces the charging effects. Details on preparing the beads for the FIB-SEM is found in section 4.4 *'Guidelines on how to use FIB on biological samples and biomaterials at NTNU NanoLab'*.

3.1.2 Cutting geometry - beads

To retrieve 3D data from the alginate beads, a practical cutting geometry was necessary. A U-trench was sputtered away on the top of the beads surface, as seen in figure 15. This approach was adopted from De Winter *et al.* [37] to avoid artefacts like shadowing and brightness effects. Several cuts needed to be done to find the appropriate parameters for soft alginate beads. An ion beam current of 6.5 nA with an acceleration potential of 30 kV was used for the rough cuts given that the dimensions of the trench was big enough; Region of interest (ROI) 10 - 15 μm wide and long (see figure 15). A clearance of 10 μm from the ROI was made to give enough space to be able to view the cross-section.
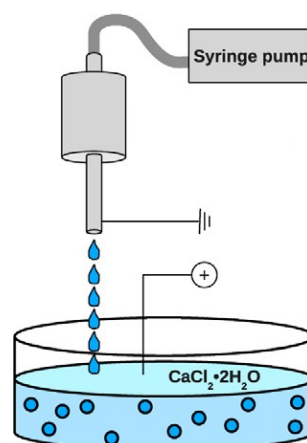

Figure 13: Illustration of how the alginate beads are made with an electrostatic bead generator. The alginate solution is dripped though a needle and in to a solution containing calcium. Gel beads a formed when the droplets hits the solution [36].
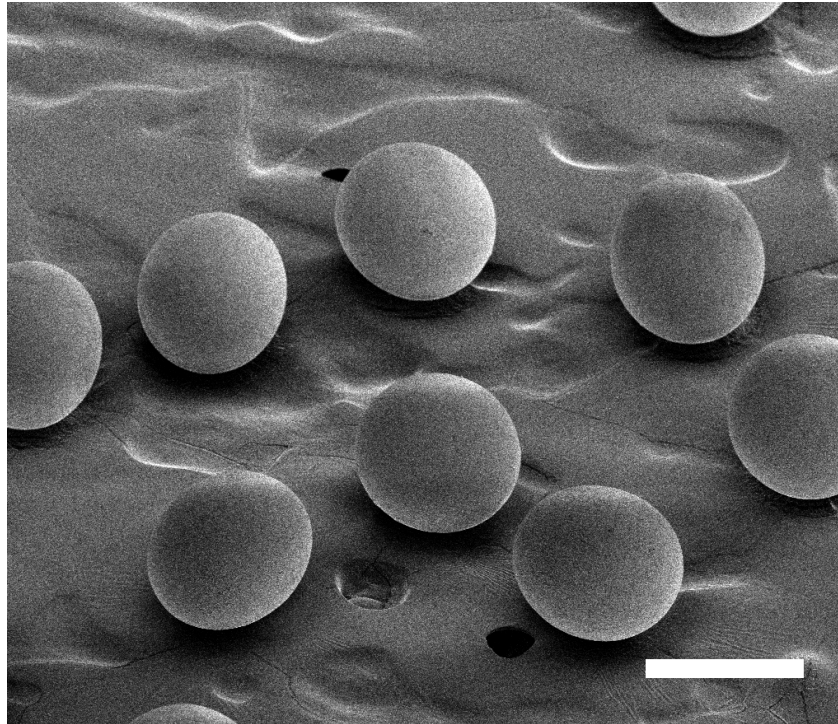
Figure 14: A SEM image of critical point dried alginate beads. The scale bar is 200 um.
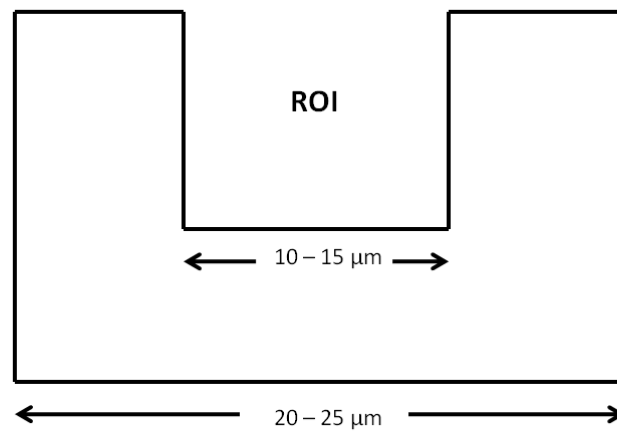

Figure 15: A schematic illustration of the cutting dimensions found to be appropriate for the U-trench for the beads.

3.1.3 Preparation of cell samples for FIB

Cells with bacteria where provided by Øyvind Halaas at The Department of Cancer Research and Molecular Medicine, as part of his research project on contributing to

find a successful vaccine for tuberculosis. The samples were prepared by Engineer Nan E. Tostrup Skogaker from The Department of Laboratory Medicine, Children's and Women's Health at The Faculty of Medicine, NTNU. The preparation procedure can be summarized as follows:

Macrophages from mouse infested with the bacteria, *mycobacterium avium*, were trypsinated and washed with PBS buffer. The cells were then centrifuged at ~ 1800 g in a test tube with a rounded bottom. After the supernatant is removed, the cells where fixated with 2% glutaraldhyd (GA) for one day. At this point, it is fairly easy to handle the firm cell pellet - cutting it in appropriate sizes (max. 1×1 mm).

Further treatment requires washing the the cells with a phosphate buffer twice for 10 min (2×10 min). To get enough material density contrast in the material, it is necessary to block-stain with uranyl acetate (UA). To further increase the contrast, especially in cell membranes, the cells were fixated again with osmium tetroxid(OsO_4), mixed with 1.5% potassium hexacyanoferrat(II)-3-hydrate. A solution of 3% potassium hexacyanoferrat(II)-3-hydrate in water was made and mixed with OsO_4 in a phosphate buffer (1:1). The cells were fixed in this solution for 2 hours and then washed in sterilized water 2×15 min. After washing the cells in 50% alcohol, the cells were added UA a second time (4% in 50% alcohol) for 30 min. Finally, the sample was dehydrated and embedded in epoxy. The final geometric shape of the sample is a block with a block face of appox. 1×1 mm as seen in figure 16. The block face is also microtomed to ensure a 'smooth' face. It is also important that the cells are positioned at the top surface and at the block face. This is to make the region of interest (ROI) more accessible and easier to set the milling configurations, which is discussed later.

Alternative staining of mycobacteria

Another staining procedure was tried, very similar to the procedure described above, where staining chemicals were added to enhance the contrast of mycobacterium avium. The procedure was done as follows:

The cells were washed with a PBS buffer and which was pipetted out. Pre-fixation with 0.075% Rutenium red, 75 nM lysine, 2.5% GA in 0.1 M HEPES for 20 min, was done. The pre-fix was pipetted out. The fixation was done with 0.0075% Rutenium red, 2.5% GA in 0.1 M HEPES for 2 hours, then washed 3 times for 10 min in HEPES buffer. The solution was centrifuged and the supernatant was removed so that $\sim$1.5 ml was left. The cells were dissolved and transferred to an eppendorf tube. Then the cells were centrifuged at 10 g for 6 mion. The supernatant was removed and hot gelatin was added.

The eppendorf tube was left in an oven for appox. 15-20 min at 40°C. Another centrifuge was done before the eppendorf tube was again left in the oven at 40°C. Redundant gelatin was removed and the eppendorf tube was cooled. The cells were post-fixated with glutaraldehyd for a minimum of 30 min and then washed with HEPES buffer twice for 15 min. The ependorf tube was cut closer to the cell pellet with a scalpel. The pellet was cut in appropriate pieces (max. 1×1 mm^3) and carefully placed in a HEPES buffer. A solution was prepared with 3% potassium hexacyanoferrat(II)-3-hydrate in water mixed with 4% osmium tetroxide in 0.1 M in HEPES buffer 1:1, where the cell pellets were post-fixated for 2 hours. Then the pellets were washed in sterilized water twice for 15 min and gradually dehydrated with alcohol (50%, 70% and 80%). 2% uranyl acetate with $\sim 80\%$ alcohol was added for contrasting at 60°C and then washed with $\sim 80\%$ alcohol 3-4 times fro 5 min. The pellets were dehydrated in 90% alcohol for 10 min, 100% alcohol 4 times for 15 min and propylen oxide twice for 15 min, and finally embedded in epoxy. 10 ml epoxy was added 0.15 ml DMP-30 (2,4,6-tris(dimethylaminomethyl)phenol) and polymerized at 60°C for 3 days.

3.1.4   Ion Beam Induced Deposition (IBID) of Platinum (Pt)

Deposition of Pt is done inside the vacuum chamber by introducing a precursor gas close to the surface of interest. The precursor is introduced by mechanically inserting a nozzle close to the sample. The gas will be absorbed on the surface and will be decomposed into volatile and non-volatile products by the incident ion beam. The non-volatile products will remain on the surface, producing deposition layers, while volatile products leave the surface [15]. In this case, the precursor gas is (ethylcyclopentadienyl)trimethyl platinum.

3.2   FIB-SEM instrument features

3.2.1   Instrument hardware overview

A FEI Helios NanoLab $^{\text{TM}}$ Dualbeam$^{\text{TM}}$ at NTNU Nanolab was used to conduct all experiments. Figure 17, 18 and 19 shows images of the instrument with the operational control system.
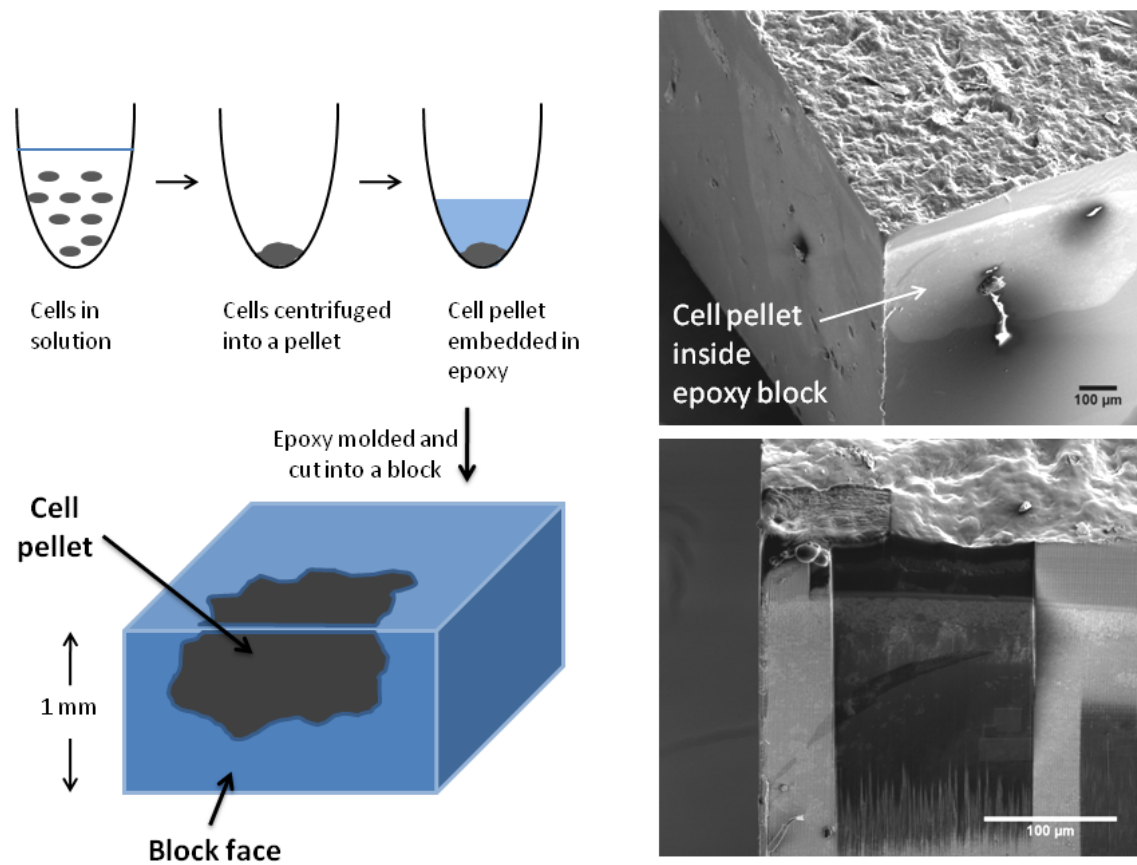
Figure 16: *Upper left:* A simplified schematic of the steps of how the cell pellet is made by centrifuge and epoxy embedding. *Lower left:* Schematic illustration of a moulded and cut epoxy resin FIB block, where the cells are exposed both at the top surface and at the block face. *Top right:* SEM image of FIB block with the cell pellet inside (white arrow). *Bottom right:* SEM image of block face where an area of the Pt/Pd layer is sputtered away to expose cells.
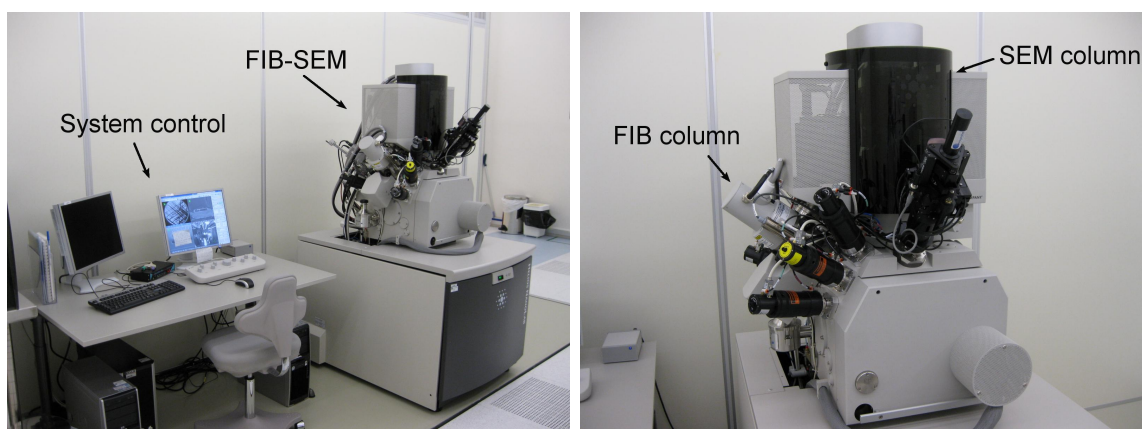

Figure 17: An overview of the entire FIB-SEM instrument. The arrows in the right picture indicates where the FIB and SEM column are placed and corresponds to the FIB-SEM schematic in figure 7.
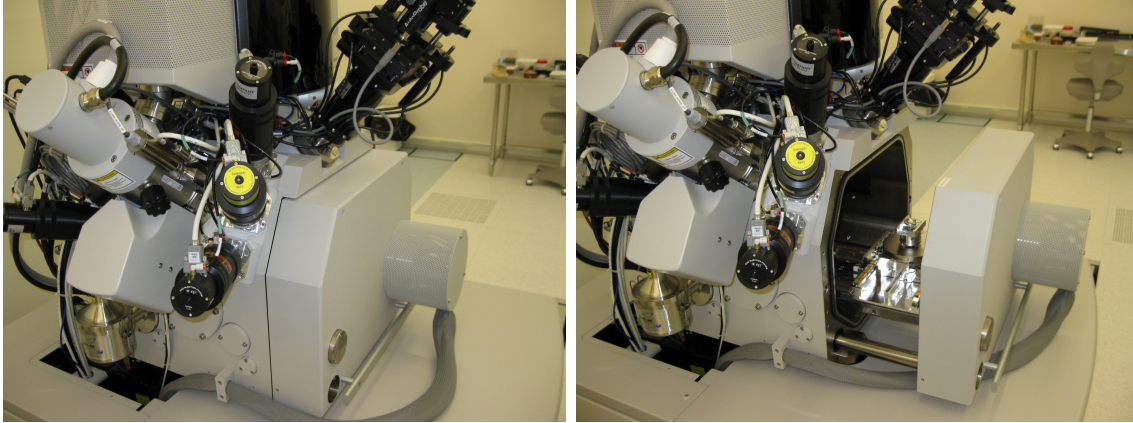
26

Figure 18: Picture of how the vacuum chamber opens and exposes the stage where the sample holder is mounted.
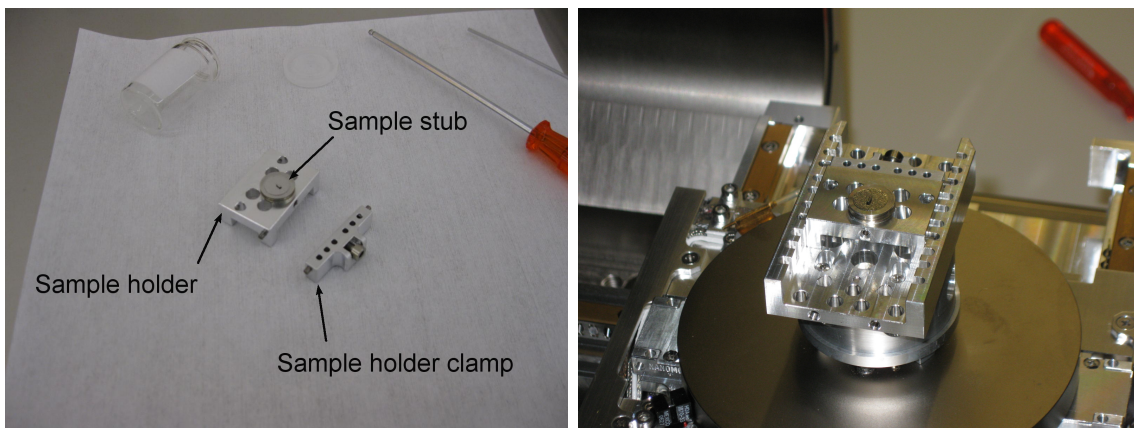

Figure 19: *Left:* Sample stub placed in the the sample holder. *Right:* Sample holder placed on the stage in the vacuum chamber

3.2.2   FIB-SEM software interface

The software interface for the control system displays 4 quads where live image from the electron beam, ion beam and an infrared (IR) camera can be observed (3 quads are mostly used), as seen in figure 20. The IR camera allows to continuously know the status inside the vacuum chamber; monitoring the stage (rotating and tilting operations) and other instrument-sample interactions, to avoid any mishaps, like physically touching the sample.
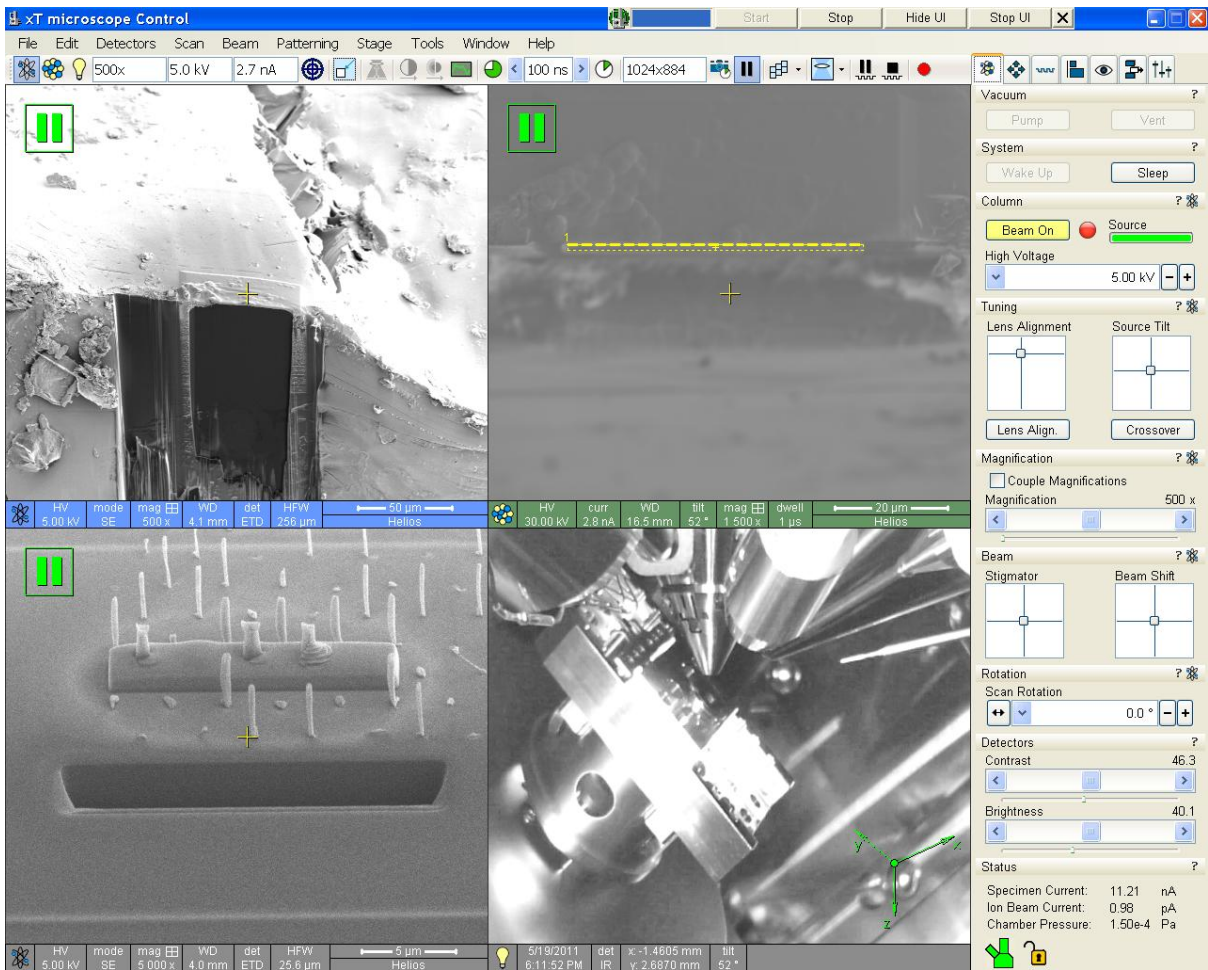
Figure 20: The image is a 'print screen' from the software interface of the control system of the FEI Helios NanoLab ^{TM} Dualbeam^{TM}. There are 4 quads where the images from the electron beam (top left), ion beam (top right) and an IR camera (lower right) are displayed (the lower left quad is redundant in this case). Surrounding the quads above and to the left are tool bars which controls different instrument settings (see figure 21).
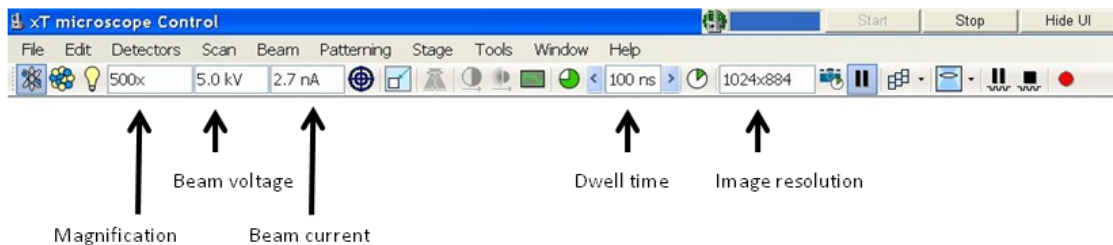

Figure 21: Tool bar in the software interface where parameters like magnification, beam voltage, beam current, dweel time per pixel and image resolution can be controlled.

3.3 Image acquisition

FEI Slice & View G2 is the software designed for the FIB-SEM to automatically retrieve 3D data. Figure 22 illustrates how the image acquisition is conducted. The electron beam observes each new exposed cross-section as each slice is milled away, and collects an image stack containing 3D data. A detailed description of how to set up the slice-and-view is explained for both samples in section 4.4, *'Guidelines on how to use FIB on biological samples and biomaterials at NTNU NanoLab'*. The guidelines suggests appropriate parameters and brings attention to the practical aspects of the instrument.

Due to sample drift[i] during the slice-and-view process, the resulting image stack needed to be aligned. This was done by using ImageJ software; *turboreg* and *stackreg* plug-ins [38]. All images of cells have been inverted to resemble conventional TEM images of cells, except in figure 31. The following parameters in section 3.3.1 and 3.3.2 were found by testing the different settings and choosing the ones that appear most suitable.

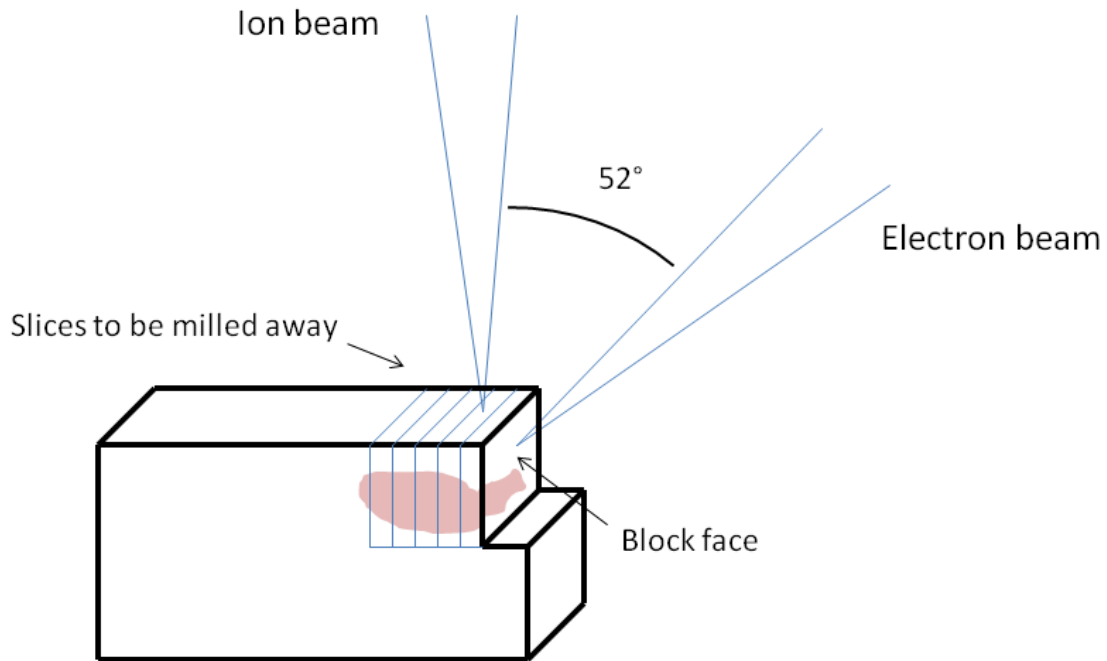[i]Unintentional movement of the sample during image acquisition.

Figure 22: Schematic representation of the slice & view setup. The ion beam and electron beam are placed at a 52° angle relative to each other. The Slice & View-software is programmed to mill away a slice and then acquire a SEM image of the exposed cross-section as the block face. Alternating between the two processes results in an image stack with data containing information in 3 dimensions.

3.3.1 Imaging conditions for slice & view for dried mineralized alginate beads

Images were acquired with 5 kV acceleration potential, 21 pA electron beam current and a dwell time of 30 μs per pixel. The images of the beads are of 1024×884, at a magnification of ×65 000. Each image was acquired at a rate of 30 s per image. The volume of stack is 2.86 μm^3 (*Alginate.avi*) (See supporting information). The stack collected consist of 80 slices, meaning a total time (including milling time of ~10 s per slice) was 30 - 45 min.

3.3.2 Imaging conditions for slice & view for stained cells

Images were acquired with a 5 kV acceleration potential, 2.7 nA electron beam current and a dwell time of 100 μs per pixel. A high dwell time was needed to detect a sufficient signal from the cross-sections. The cell image stacks in this study are of 2048×1887 pixels,

at magnifications between $\times 5\,000$ and $\times 8\,000$. Each image was acquired at a rate of 6.5 min per image. The volume of stacks are 122.36 μm^3 (*Macrophage1.avi*), 2508.37 μm^3 (*Macrophage2.avi*) and 2715.60 μm^3 (*Bacteria.avi*)(See supporting information). The stacks collected consists of 96, 277 and 244 slices, respectively, meaning that total time (including milling time ~ 1 min per slice) was approx. 12, 36 and 30 hours.

In the case of the cell image stacks, they needed further treatment. Three cell image stacks in video clip format, are attached to this project (see Supporting information), *Macrophage1.avi*, *Macrophage2.avi* and *Bacteria.avi*. The image processing was done using ImageJ inverter and FFT Bandpass filter (however, filtering was not done on *Bacteria.avi*). The bandpass filter is used to remove edge artefacts as it removes high spatial frequencies (noise) and low spatial frequencies (small variations in signal detection), thus optimizing the signal-to-noise ratio. Also, the filter suppresses horizontal or vertical stripes [39]. Appropriate parameters chosen for the filter-treated cell images were; 'Filter Large Structures' down to 100 pixels and 'Filter Small Structures' up to 3 pixels for. The brightness and contrast of the images where adjusted to an appropriate level.

4 Results and Discussion

The focus of the project has been to gain an initial competence in how the FIB-SEM should be utilized in order to acquire structural information from samples in three dimensions. This involves studying the sample geometry, the interaction between the ion beam and the sample material, and comparing electron signals and detectors. Here two different materials were studied.

4.1 Critical point dried hydrogel beads made of Ca-mineralized alginate

4.1.1 Region of interest preparation

The hydrogel beads are used in tissue engineering as they are used to encapsulate cells and promote cell growth. Because of the beads high porosity and high water content (96%), the material is soft and becomes structurally weak and brittle when dried. No literature exists on how to treat the beads or how the beads would interact with the FIB. As described earlier, to retrieve structural information in 3 dimensions a strategy from De Winter *et al.* was adopted, where a U-shaped trench is sputtered away leaving a region of interest (ROI) exposed. When the ROI is exposed in this way, it will reduce shadowing or brightness gradients at the imaging face [37]. At the early stages, a trial-and-error strategy was conducted. Figure 23 show how the trench looked like using a low ion beam acceleration voltage (5 kV) and when too small trenches were used. The figure also gives an impression of the porosity and structural weakness of the dried gel as a great deal of damage is done to areas other than intended. In both images in figure 23, the ROI is severely altered from its original state. However, when the dimensions of the trench were increased (as in figure 15) the trench became much more defined as it is thought that the increase in size also increases the structural strength and integrity of the porous material. Figure 24 shows a structurally stable trench where further sputtering can be done in a more controlled and tidy manner. The U-trench is considered a 'rough cut', designed as a suitable workplace for further investigation of the ROI.

4.1.2 Curtaining

Prior to setting up the slice-and-view process, it is important to find a good cutting current that will leave the original dried hydrogel structure as intact as possible. According to Knott *et al.*, depositing a protective platinum layer on the top surface before cutting,
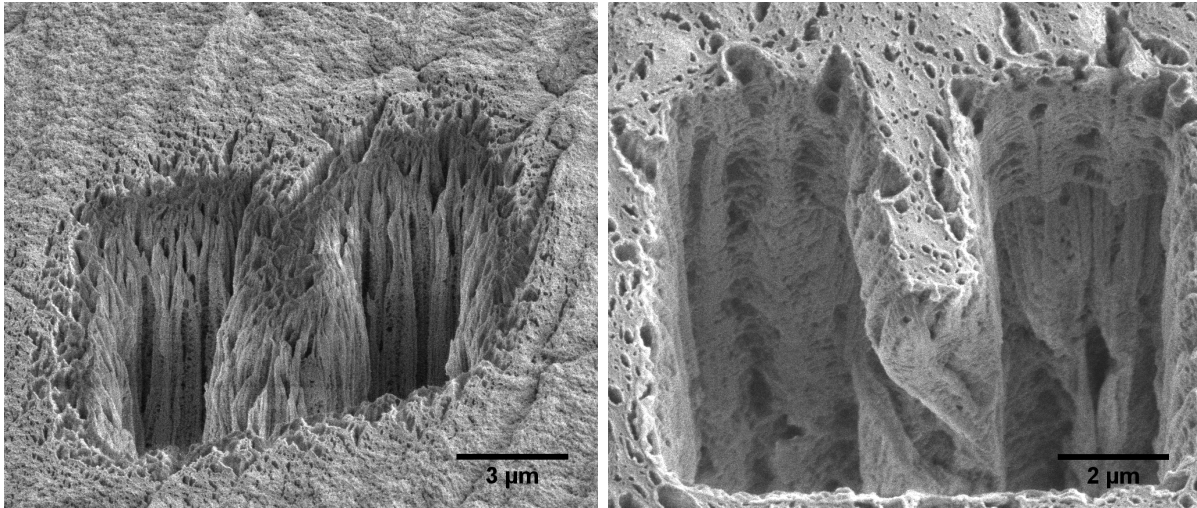
Figure 23: SEM images of early stage U-shaped trenches. Parameters used for the acceleration voltage and the ion beam current are 5 kV and 1 nA (left), and 30 kV and 6.5 nA (right).

will ensure that the face is milled more evenly and remains parallel to the direction of the ion beam [21]. Due to sample topography (uneven top surface) or material differences, there will be excessive streaking or vertical stripes down the block face induced by the ion beam, called curtaining, as seen at the top in the left image in figure 25 [40]. The deposited Pt-layer help to reduce this effect. In the case of the beads, it is evident that the curtaining becomes more protruding further down from the top surface, as seen to the right in figure 25. For this reason the images were collected immediately below the Pt-layer, where no curtaining effects could be observed (see figure 26).

4.1.3 3D data

In figure 27 shows 10 subsequent SEM images being a part of a larger image stack (See supporting information: *Alginate.avi*). These images show how the structure through the pores in the dried alginate bead changes for each slice. The slice thickness here is 25 nm. The entire stack collected gave a total volume of (need to find volume). Although, the data needed to do a three dimensional reconstruction of the beads is already acquired, the images need processing, *e.g.* threshold adjustment. By binarizing the bead cross-section images, making the voids black and the structure white, it would be easier for the reconstruction software to interpolate such a simplified image stack. Also, to get the most accurate reconstruction as possible, the contrast variations of the structures need a more complex image processing. Due to the topography contrast, features that are present in a slice, may also be present in the proceeding slice even after a section is milled away. This will disturb the resolution in the z-direction and, thus, need further processing to
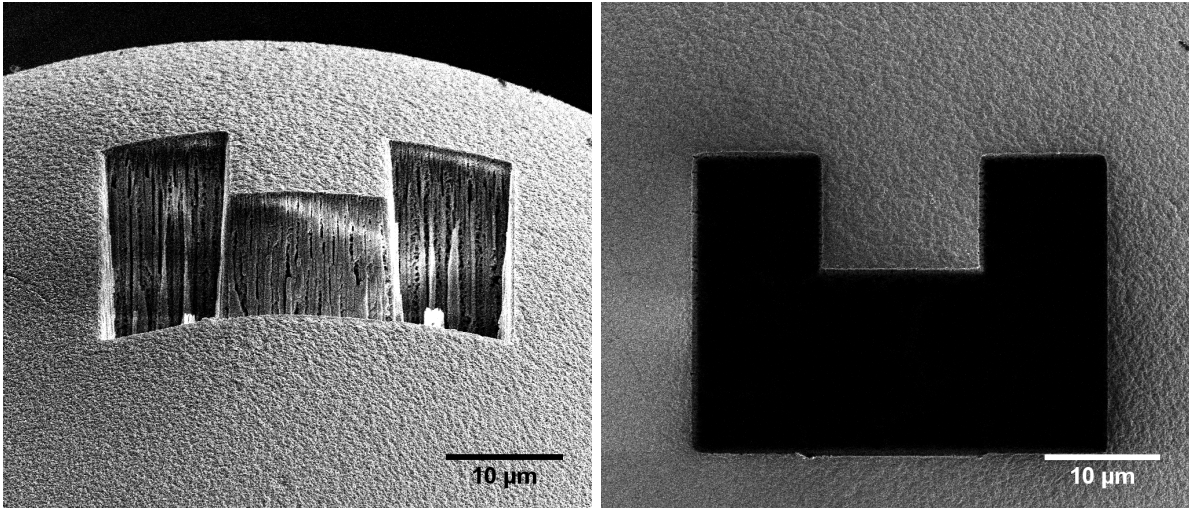
Figure 24: SEM images of a successfully cut U-trench on the bead surface with acceleration voltage of 30 kV and an ion beam current of 6.5 nA.

obtain an improved resolution. Such image processing has not been attempted in this project.
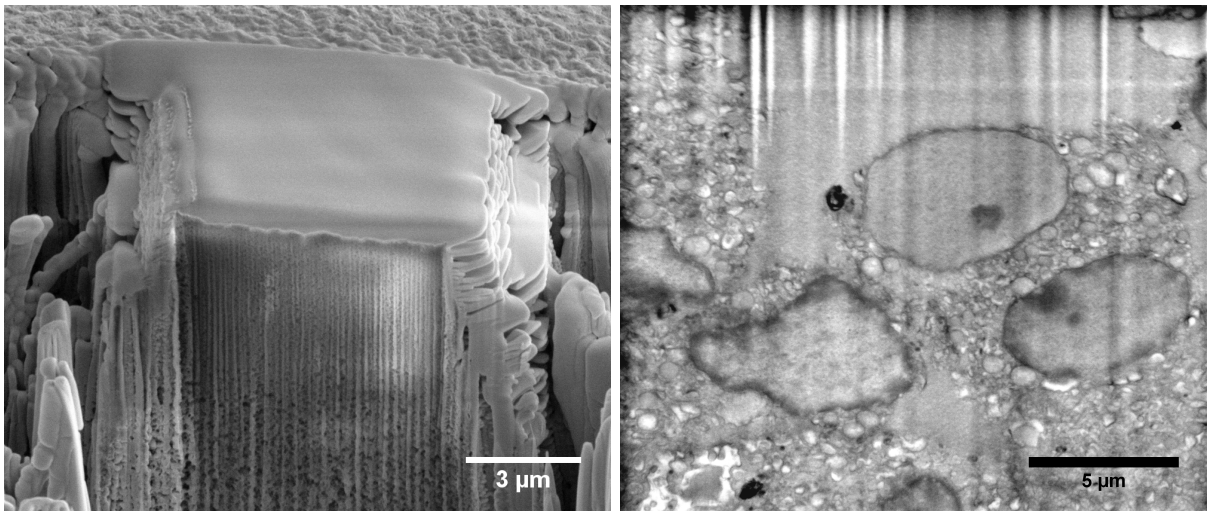

Figure 25: *Left:*Region of interest standing where an ~ 0.75 μm thick layer of Pt is deposited at the top surface using ion beam-induced deposition (IBID). Clearly the curtaining can be observed further down from the top surface. *Right:* Curtaining effect is observed at the top of the image.
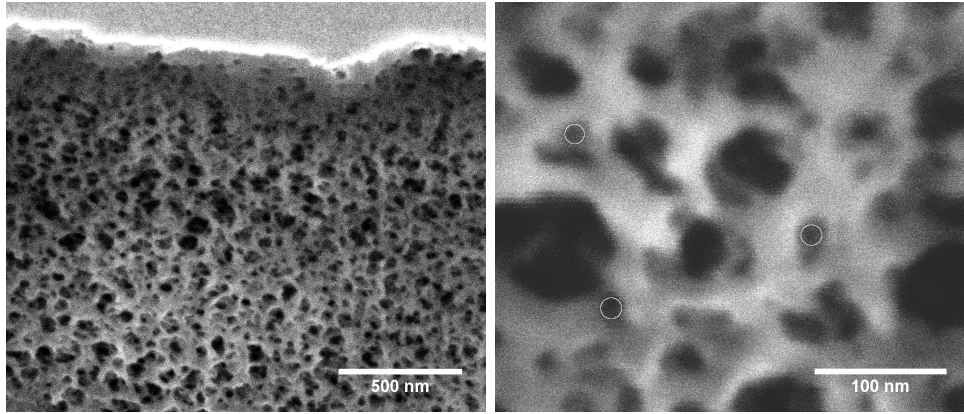
Figure 26: SEM images show cross-section of the region of interest sputtered with the ion beam with 30 kV and 2.8 nA. At the top of the left image the platinum layer can be seen. Immediately below this layer there are no curtaining effects and therefore the optimal place to retrieve structural information. The smallest resolved structures are around 10 nm observed in the right image (marked with circles).
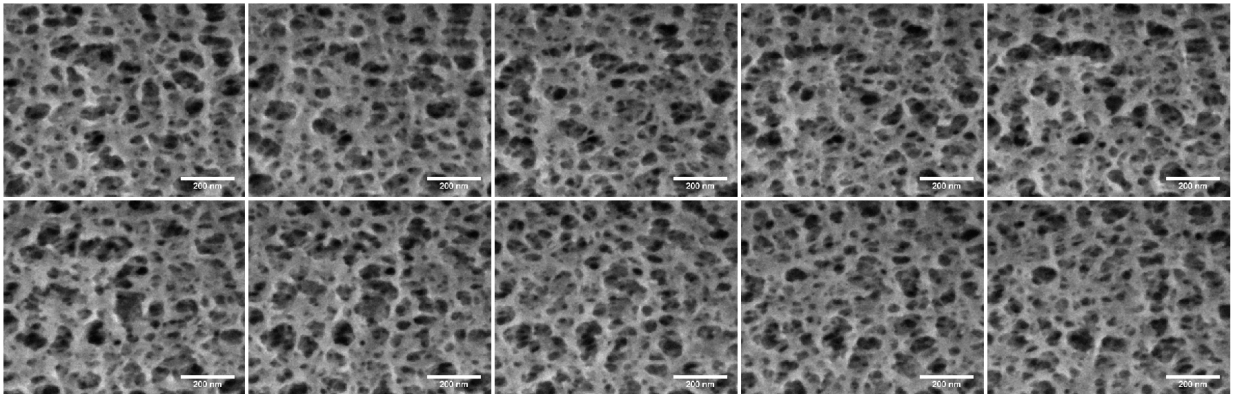

Figure 27: A montage of the interior structure of a alginate hydrogel bead showing 10 cross-sections (upper left to lower right). The distance between each cross-section is 25 nm. The scale bar is 200 nm.

4.1.4 Further progress

At this point, the only part of the bead which have been investigated, is the surface and immediately beneath the surface ($\sim 2~\mu$m). Since the intention of the alginate beads is to encapsulate living cells, it is important to also be able to characterize deeper within the bead. By looking at figure 25, it is evident that the curtaining effects are very strong deeper in the biopolymer material. Conducting an accurate analysis deeper in the bead, would be a difficult task if the same 'U-trench'-strategy is used. The cross-sections would

35

simply be to different from its original state, and also the trench would need to have much larger dimensions to avoid loosing signal from the sample. The main challenge arises from the porosity and the softness of the bead, which makes it unlikely to access the center of a bead just by milling a large trench, without destroying large parts of the bead.

4.2 Epoxy resin embedded cells

4.2.1 Region of interest preparation

The first attempt with biological samples were macrophages from mouse infested with mycobacterium avium, made into a cell pellet, embedded in epoxy resin and moulded into a TEM-mould, as seen in figure 28. Epoxy is a dense plastic material and is much more stable than the dried alginate beads.

The first images acquired of cells in the TEM-mould are shown in figure 31. Since the cells in the resin are not sufficiently stained (because the cells lack uranyl acetate (UA) staining as these samples are post-stained after they are microtomed from the mould), the cells will display a poor contrast. Some cellular features are still visible since they were fixed with OsO_4, but no way near good enough to support a proper reconstruction.

The cells are intendedly placed at the top surface to be able to microtome thin slices for use in TEM. The epoxy mould (in this case modified in size to fit the vacuum chamber) was mounted on the stage in the FIB-SEM, with the region of interest (ROI) containing cell material facing up, so the electron beam hits the top surface perpendicularly. The ion beam is placed at an 52° angle relative to the electron beam (see figure 7) and the stage is able to tilt between 0° and 52°, following the same arc that stretches between the FIB and the SEM. This means that it is only possible to make cuts between 0° (perpendicular) and 52°. So having the surface of interest faced up, is a somewhat impractical set up if the goal is to retrieve 3D data from slice-and-view. Although, it would be possible to follow the same cutting strategy as for the beads (milling a U-trench), but, as mentioned, epoxy is a much more robust material (heavily crosslinked polymer [41]) and it would take more time to cut out a sufficient U-trench witch is deep enough and has well defined edges. This was attempted in an experiment shown in figure 29. Here it is evident that when making a rough cut of this kind, with very high ion beam currents (*e.g.* 21 nA) there will be higher amounts of re-deposition[j], making the cut and the walls uneven. The U-trench would need further milling at low ion beam current (also referred to as polishing) which

---

[j]Depostion of material that is already been sputtered away.

also takes more time.

Another approach to access the cells beneath the surface, was to cut a V-like trench with each side wall at a 45° angle as done in the left image in figure 30, and in this way be able to image the cross-section perpendicularly. But still, this is an impractical strategy to collect image stacks. This would result in milling out a hole in the sample that would become too deep, and eventually loosing electron signal as the electrons will have difficulty in reaching the detector.
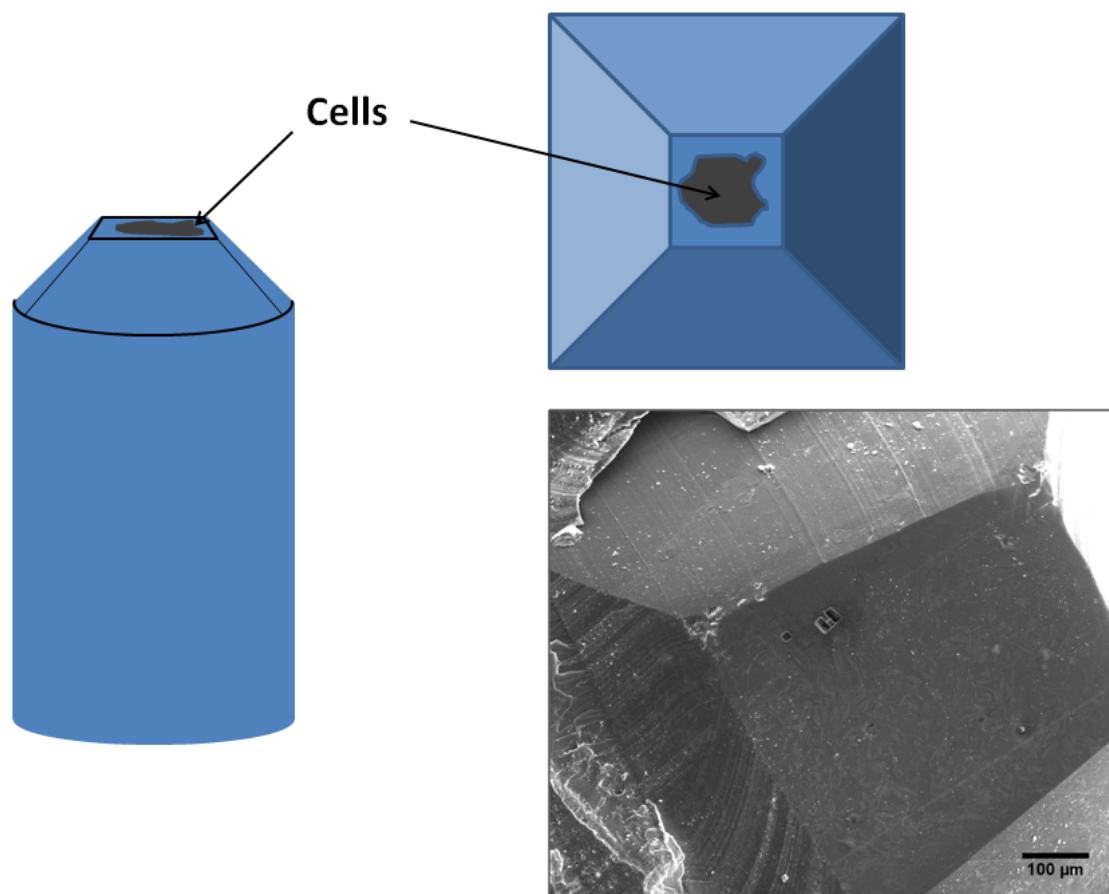

Figure 28: Left and top right shows a schematic illustration of a TEM mould, where the left image is a side view and the top right is a top view. Lower right is a SEM image of the top view.
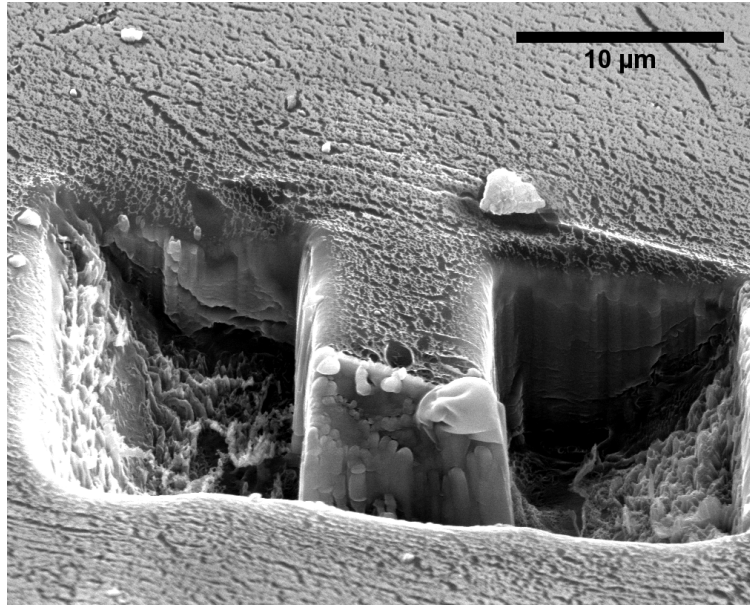
Figure 29: A SEM image of a U-trench cut in epoxy resin with a high ion beam current (21 nA) at 30 kV. There are heavy traces of re-deposition at the walls making this a very rough cut which need further polishing to become a sufficient trench with 'clean' walls.
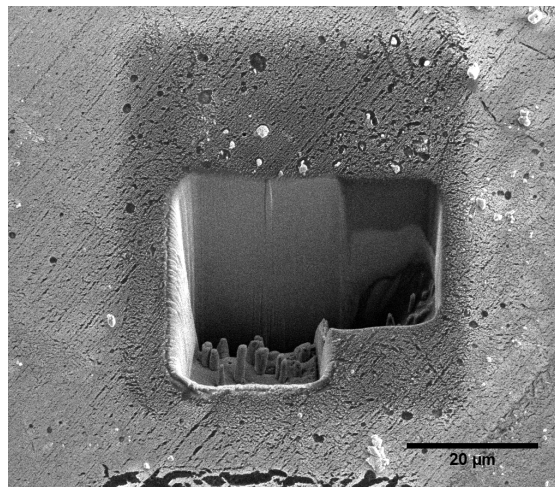

Figure 30: A trench cut out in epoxy TEM pellet at a 45° angle to be able to view the cross-section perpendicularly.
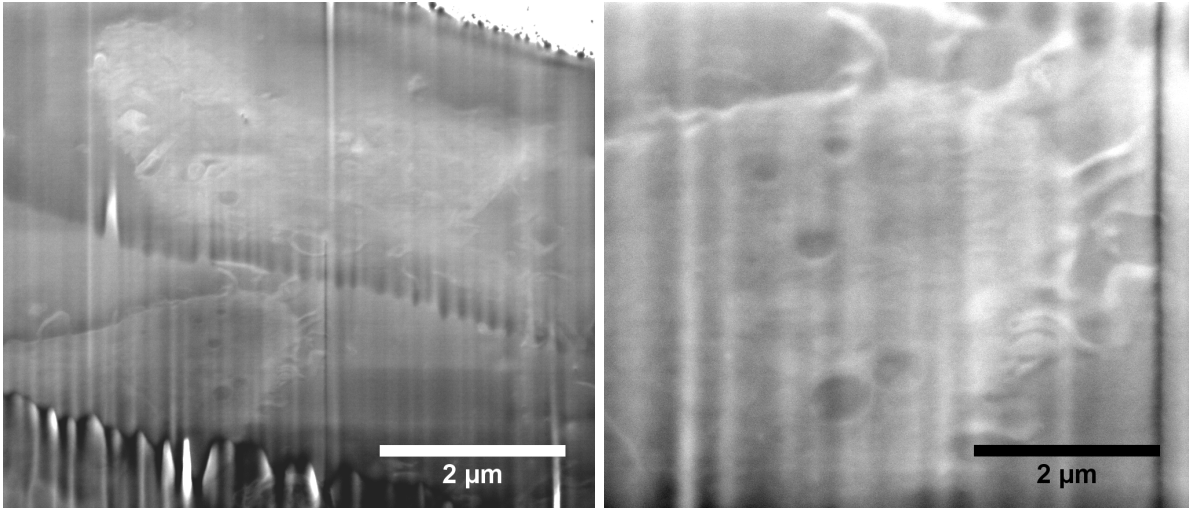
Figure 31: SEM images of a cell in a TEM pellet. Preparation steps, in this case, for the TEM-samples include microtoming thin slices (sub 100 nm) and post-staining the slices with uranyl acetate before placed in the TEM-sample holder. This sample is therefore not sufficiently stained.

4.2.2 Geometry of the FIB-block

When setting up the slice-and-view, the region of interest (ROI) needs to be in a state where the cutting conditions are the same throughout the whole process; same cutting angle (ion beam and top surface perpendicular to each other) and same viewing angle (52°). Also, as the slicing cuts deeper into the sample, it is advisable to have the cross-sections larger than the actual ROI that is being imaged to avoid any shadowing and loss of signal in the collected stack (this is one of the advantages with the U-trench). In 2008, Knott *et al.* introduced a block geometry of the FIB-sample. Making sure that the cells where both exposed at the top surface *and* the block face (see figure 16 and figure 32*f)*) ensured a stable condition while doing slice-and-view, with respect to constant geometry angles.

Figure 32 illustrates different issues of FIB-blocks, which have been tried to collect images from. In figure 32*a)* and *b)* the placement of the cells introduce a problem if the distance of the cells exceed ~ 20 μm from the edge of the the top surface and the block face. For the case of 32*a)*, as the distance increases the curtaining will become more severe. The further down the cells are, the more pronounced the curtaining will appear after milling. Another way of reducing curtaining effect other than depositing a Pt-layer at the top surface, is to use a lower ion beam current. However, this will increase the milling time. In this study of epoxy embedded cells, a current of 0.92 nA was used to mill

the cross-sections as it appeared suitable for milling depths down to ~ 20 μm without experiencing any severe curtaining. In figure 32b), one would have to mill away a great deal of 'empty' material to expose the cells, which is an unnecessary use of time, when the cells can be placed at the edge ready for slice-and-view. In figure 32c) both incidents from a) and b) are present.

Figure 32d) displays a geometry where there is a steep angle at the cutting edge. This is inconvenient for several reasons. First of all, the eucentric height[k] will change through the slice-and view. The eucentric height is an important parameter that the software uses to auto-adjust the focusing during slice-and-view. Additionally, if the angle is too steep ($>45°$) it is thought that the ion beam will be distorted or deflected when it hits the surface and mill away the slices unevenly. Also, the total volume that is milled will have an angle (see figure 33), which limits how large the image volume collected can be as the sample would have to be moved. It is possible to image a larger area to ensure that the interesting features stay within the stack, but this will limit the image stack to a low magnification. Ideally, the edge should be a perpendicularly moulded, however a slightly inclining angle of the top surface (around 10°) can be tolerated.

Figure 32e) illustrates a rough top surface. A rough surface like this would cause and amplify these effects. Only a certain degree of roughness can be tolerated as a deposited Pt-layer is only reducing the curtaining, not eliminating. Microtoming the top surface has been sufficient enough. Figure 32f) shows the best geometry of them all, and is the geometry used for the images collected in the following sections. Figure 34 shows a SEM image of an actual block with such an geometry, with an area at the block face milled away. This is to 'scratch the surface' and expose the cells that are covered by a sputter coated layer of Pt/Pd.

---

[k]The hight that ensures that ROI is centered and focused when tilting the sample.
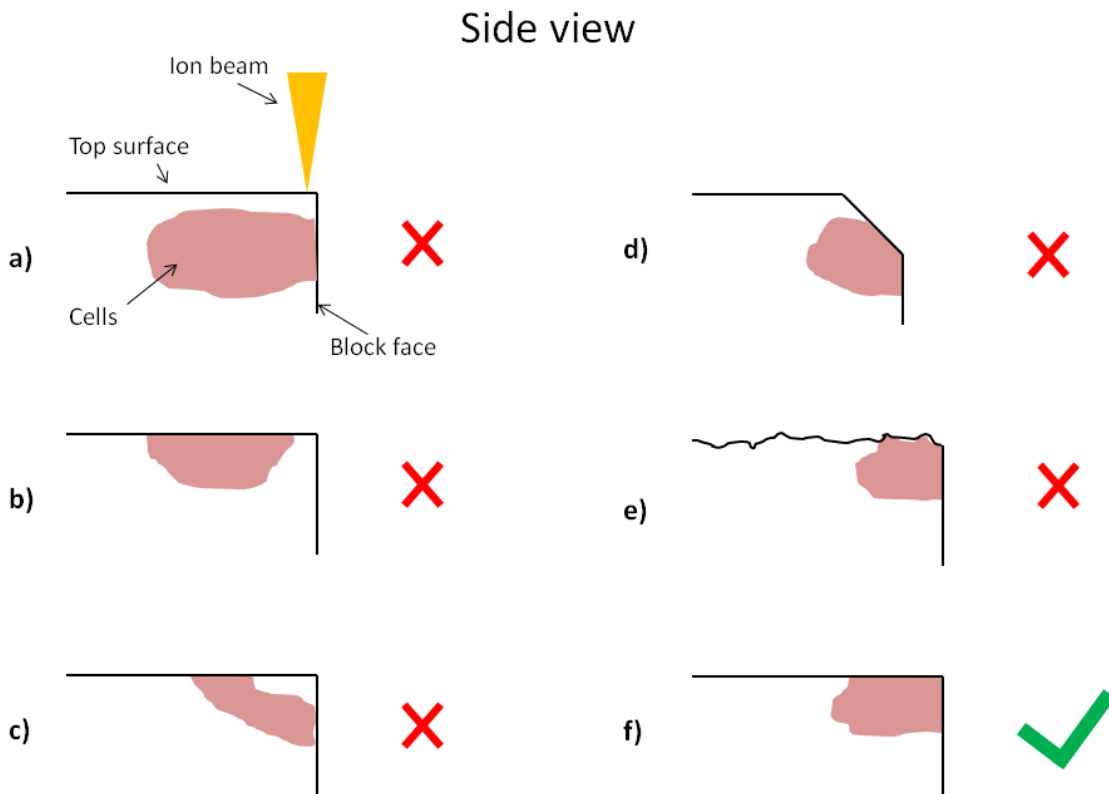
Figure 32: A schematic illustration, viewed from the side, of different geometries of the FIB block, *a)*-*f)*, that have been experimented on in terms of getting the best cuts and successfully completing a slice-and-view session. The placement of the cells in *a)* will be too far away from the top surface if the distance exceeds ~ 20 μm. At this distance vertical stripes from curtaining will obscure the image. When the cells are place further from the edge at the top surface as in *b)*, unnecessary time is spent to mill away 'empty' epoxy. In *c)* both issues in *a)* and *b)* are present. Alternative *d)* shows a steep angle at the cutting edge which will cause several implications as discussed in the above section. If the top surface is too rough, as illustrated in *e)*, unwanted curtaining effects will occur already at the immediate distance below the top surface at the cross-section. The final alternative, *f)*, has the cells placed at the very edge where the block face and top surface meet perpendicularly and represents the ideal option of them all when it comes to preforming good cuts and collecting good image stacks.
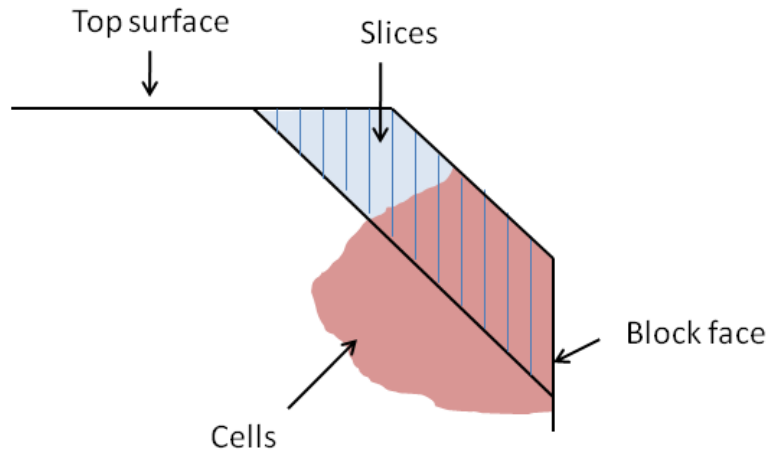
Figure 33: A more detailed illustration of alternative *d*) in figure 32 showing the total volume that will be cut.
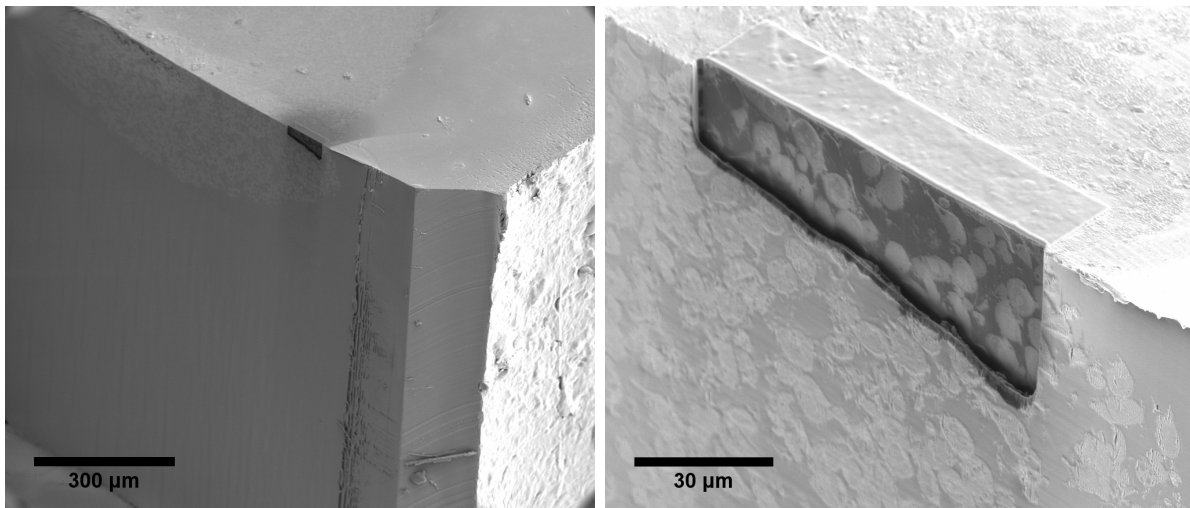

Figure 34: SEM images of a FIB block with an appropriate geometry. An area at eh block face is milled away in order to expose cells underlying the sputter coated layer of Pt/Pd. Also, Pt layer has been deposited on a smaller area at the top surface to promote smooth cross-sections and ensure even cuts. In this case, it is possible to see the limited area at the edge where the cell pellet is placed.

4.2.3 Comparing detectors and detector modes

The FIB-SEM has the ability to easily change between detectors; ETD and TLD, and change between electron signal modes: SE and BSE. In the following section a comparison of these settings has been done with the intention to find the optimal image condition.

The interior of the bead structure has a porous architecture and therefore an obvious choice to look at SE electrons as this signal is strong when the surface is heavily

characterized by topography features. Here the contrast originates from difference in the probability of the SE to escape from the surface [11]. However, when looking at epoxy embedded cells where each cross-section is completely flat, the contrast mechanism arises from the atomic number (Z) contrast. Certain elements of the cells, like membranes and vesicles have been stained with heavy elements as described in the preparation protocol (see page 23).

In the literature, there is a consistency in regards to the imaging conditions of cells embedded in epoxy. Knott *et. al* and De Winter *et. al* , both use the same strategy when acquiring a SEM image stack [21, 37]. Utilizing the TLD (also referred to as in-lens detector) they mainly detect high-energy BSE originating from the heavy elements in the stain and creating a Z-contrast. They also find that the acceleration potential for the electron beam is optimum at 2 kV. However, those parameters do not correspond to the results in this study. It is expected that the resolution would be better when lower accelerating voltages are used, because of a smaller interaction volume. If the structures are larger then the width of the interaction volume, they will not be resolvable [26]. On the other hand, the use of low accelerating voltages may not give the best images as the spot size will be wider and give a larger surface area of interaction, decreasing the resolution [26]. It is also worth considering the calibration of the SEM. If the configurations, like beam alignment, for an acceleration voltage of 5 kV is better than for 2 kV, this could make a considerable difference in image quality. From experience, it seems that with any sample the best results comes from experimentally adjusting the accelerating voltages to the value that gives the best quality/resolution.

Assuming that an good image has sufficient resolution and contrast, the findings in this project indicate that the SE mode is best configuration, almost regardless of using ETD or TLD. In figure 36 there are four images; ETD in SE (upper left) and BSE mode (upper right), and TLD in SE (lower left) and BSE mode (lower right) (all inverted and processed with FFT bandpass filter). These images are acquired during slice-and-view to avoid any unwanted built up contamination from deposition of a carbonaceous layer. At first glans it is the BSE images that have the better contrast due to the strong atomic number signal. Comparing ETD BSE and TLD BSE, and in terms of resolution, it is the TLD image that is better. This is expected since the TLD acquires a strong magnetic field to collect high-energy electrons more efficiently and handles a stronger signal (see section 2.2.1). Both SE images have better resolution than the TLD BSE. Although a worse contrast, SE images are expected to have a better resolution since the electrons originate from a smaller interaction volume than the BSE. The difference in contrast and

resolution is observed in figure 38 and in more detail in figure 39 where the signal-to-noise ratio is better for the SE image. Also, it possible to clearly see the topographical vertical lines in the SE image from the ion beam cutting. Although the contrast is not as good as the BSE image, it is still sufficient to see the cellular features. This indicates that the staining compounds and the carbon-based material of the cell and epoxy have enough difference in atomic number to produce contrast with SE (Osmium having Z=76 and Uranium Z=92)[1].

On the other hand, the two SE images are very similar in contrast and resolution, at this magnification ($\times$ 8000). The magnification is no where near the resolution limit ($\sim$ 1 nm), making it difficult to determine if the resolution is better for the TLD or the ETD. Knowing that the TLD would only detects SE_1, while the ETD would mainly detect SE_1 and SE_2, it would be expected to observe a stronger signal with the ETD. However, both detectors can be used for this type of study as there is no noticeable difference in the images. In this project the ETD was used to do the further work, simply because it is a well-known and easy-to-operate detector.

---

[1]http://www.bpc.edu/mathscience/chemistry/history_of_the_periodic_table.html
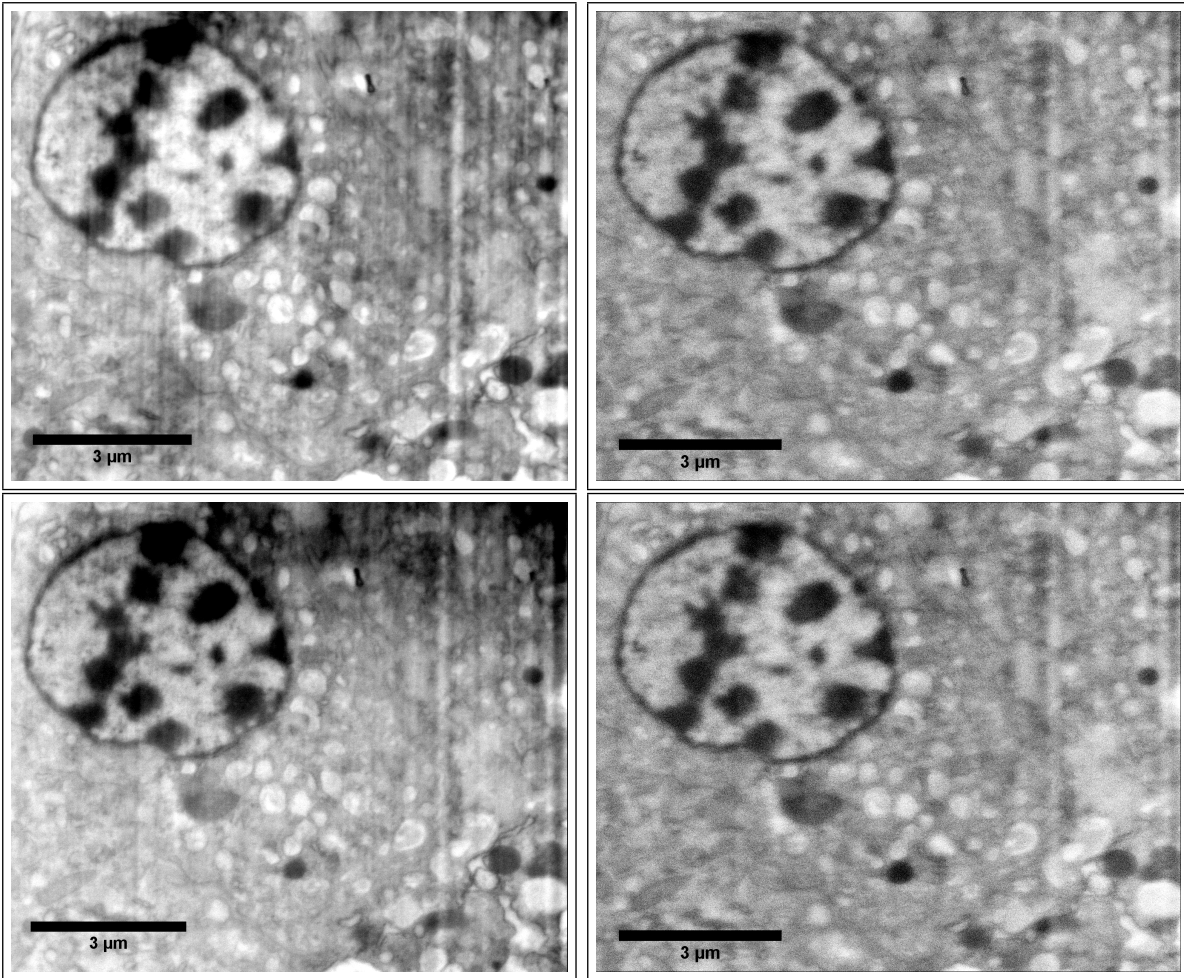
Figure 35: Four SEM images of a Macrophage cell nuclei and organelles, where each image is acquired with a ET detector or a TL detector set to SE mode or BSE mode. *Top left*: Using ETD in SE mode. *Top right*: Using ETD in BSE mode. *Lower left*: Using TLD in SE mode. *Lower right*: Using TLD in BSE mode. All images are obtained with 5 kV and 2.7 nA.
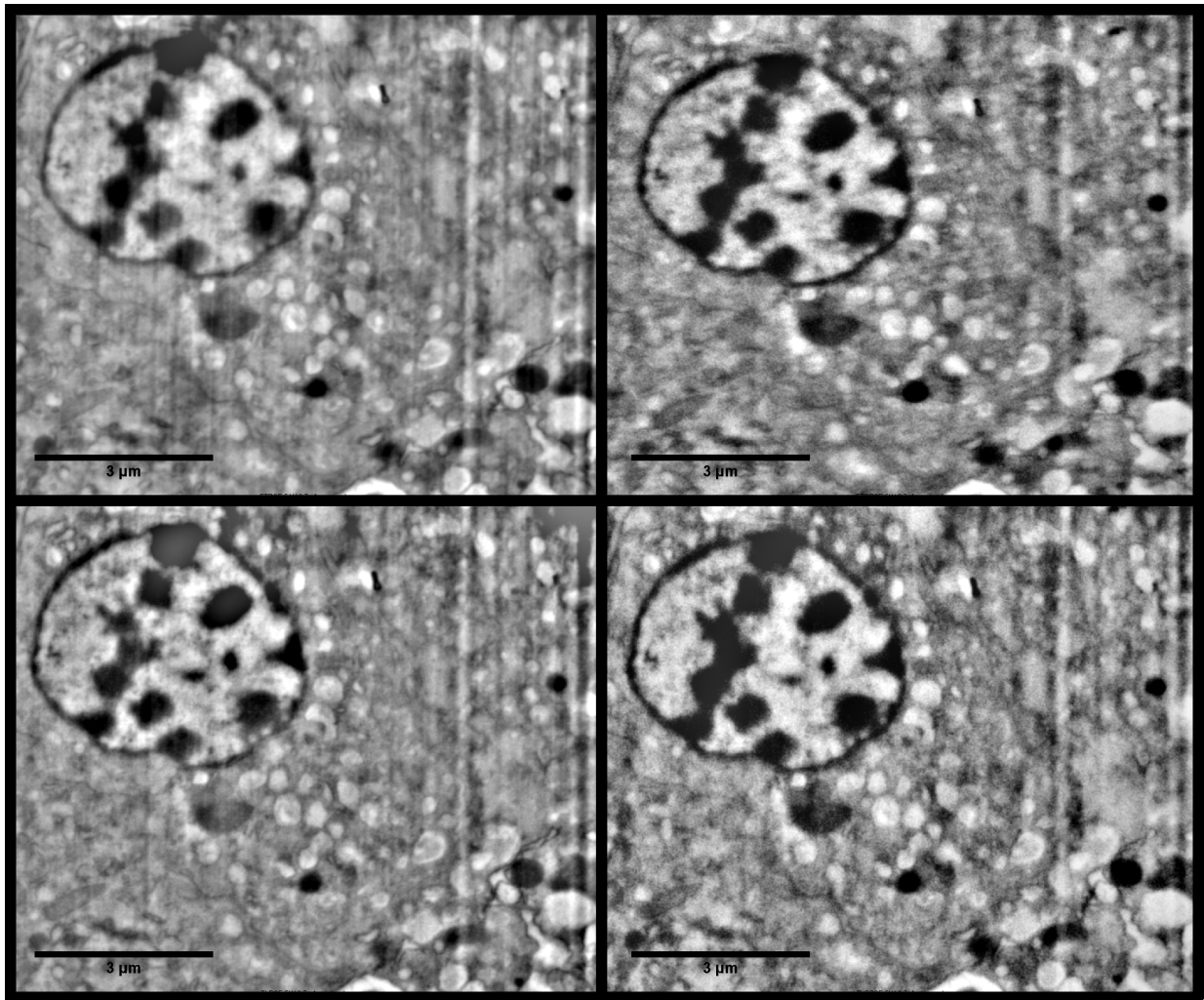
Figure 36: Same images as figure 35 but here the images have been Fast Fourier Transform (FFT) filtered.

In this study, the images are clearly are of better quality when an acceleration potential of 5 kV is used. In figure 37 three SE images of cells are acquired with three different potentials with the same beam current. The first image (top) is taken with 2 kV and displays an image that is very sensitive to the topography compared to the 5 kV image. This gives a poorer contrast as the surface features vaguely obscures the atomic number contrast. The 10 kV (bottom) image has good contrast and has less topography contrast as the penetration depth is increased with higher beam energy, but at the cost of loosing structural cell information. In the upper right corner of the images there are some ultrastructural cell features giving a strong signal. Due to the increased penetration depth and the signal originating from deeper within the sample, these features 'blur' together and makes it difficult to analyse. If high voltages would be used for collecting stacks, this would give worse resolution in the z-direction. Also, higher voltages makes

46

the sample more exposed to charging effects. In the 5 kV image (middle) the same cell features do not blur together and at the same time conserves a good contrast from the rest of the cell. No obvious charging can be seen here.
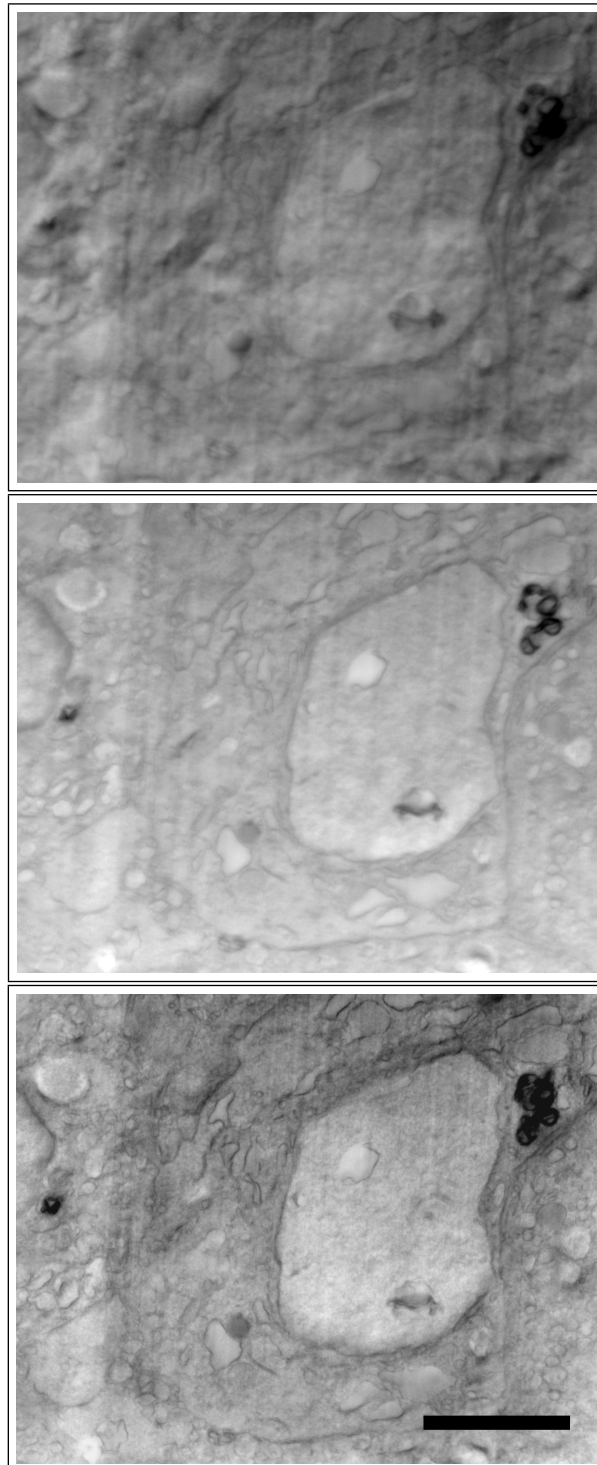

Figure 37: Three SEM images showing cell features all taken with Everhart-Thornley detector but with different voltages; 2kV, 5 kV and 10 kV (from top to bottom). The scale bar is 3 μm.
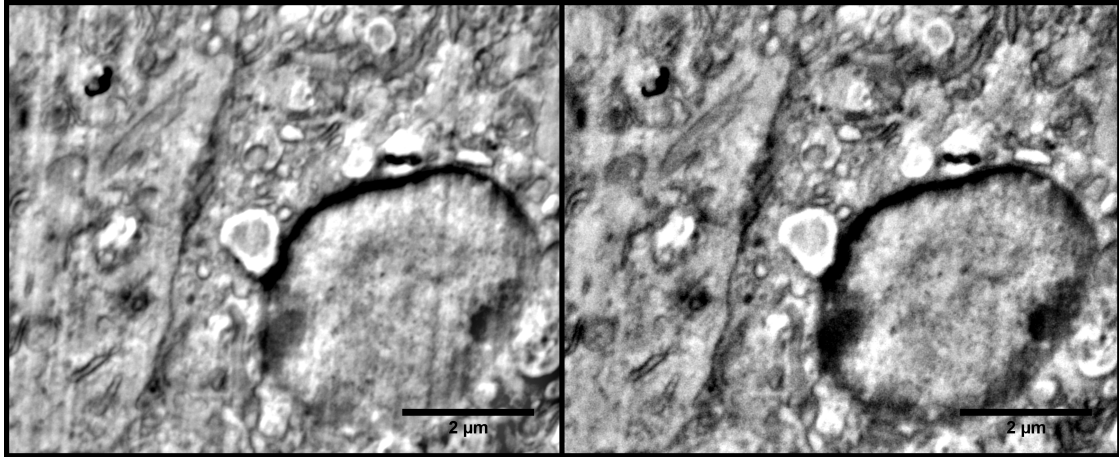
Figure 38: *Left:*Image acquired with Everhart-Thornley detector in secondary electron mode. *Right:*Image acquired with Through-lens detector in backscattered electron mode. The images show a cell where the cell nuclei and organelles can be seen.
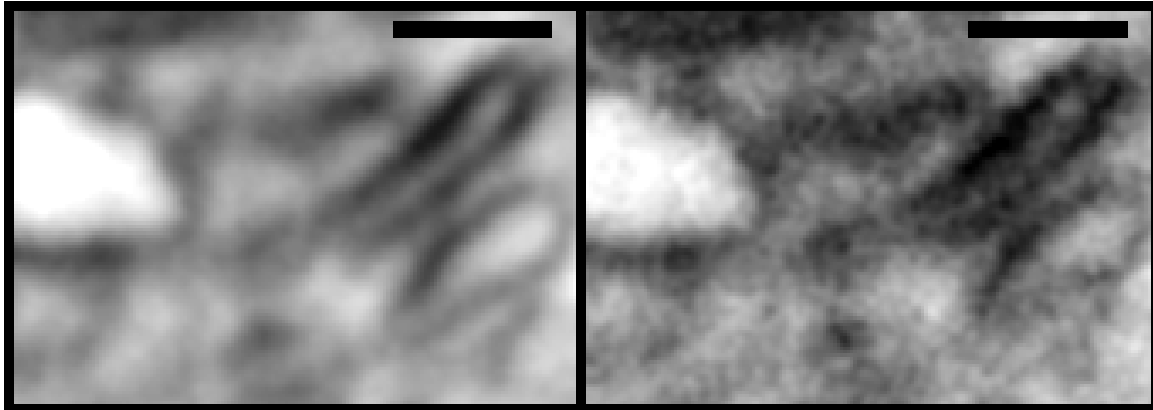

Figure 39: *Left:* Image acquired with Everhart-Thornley detector in secondary electron mode. *Right* Image acquired with Through-lens detector in backscattered electron mode. The images show a intracellular feature intended to show the difference in resolution between the two detectors. The scale bar is 250 nm

4.2.4 Comparing SEM images to simulated confocal microscopy image in 2D

As previous mentioned, CLSM is capable of acquiring image stacks and thus reconstructing the data in three dimensions. In this section, the intention is to compare a confocal image and a SEM image, and show that SEM is superior in resolution. This is done by using ImageJ and resizing an SEM image down a desired number of times and then again resizing it back to its original size, but keeping the changed information per pixel. In figure 40 the original SEM image has a magnification of 5 nm per pixel. It is assumed that the optimal resolution of an confocal microscopy image is 250 nm. By reducing the

48

SEM image 50 times, and enlarging the image 50 times, the enlarged image will have a magnification of 250 nm per pixel. The image will then resemble a confocal image in terms of resolution. It is also assumed here that the contrast in 'confocal image' and the SEM image are the same, which it usually is not. Nevertheless, the comparison gives an idea of how big the difference in resolution is.
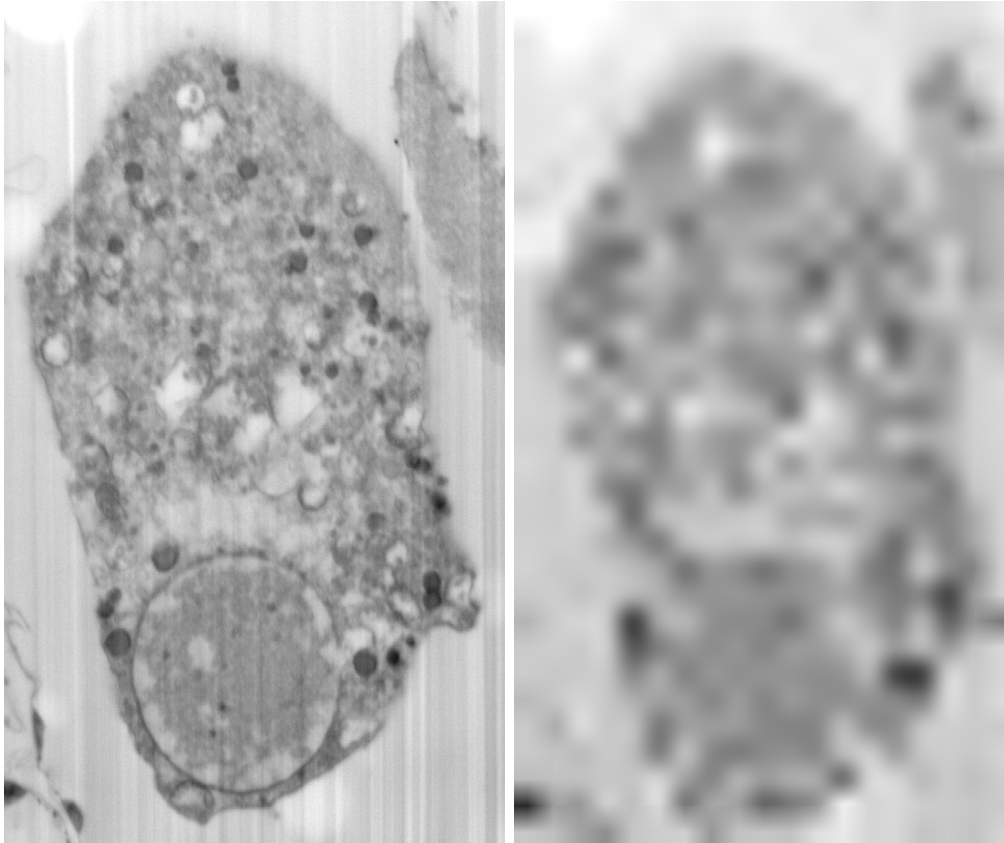

Figure 40: A comparison of a SEM image of a macrophage with a simulated confocal image of the same macrophage. The 'confocal image' is simulated by rendering the pixel values in the SEM image so that each pixel contains an estimated value that would correspond to an actual confocal image.

4.2.5 Using Fourier Transform to process images

To further improve image quality such as filtering away noise (increasing signal-to-noise ratio) Fourier Transform was used by using ImageJ software. By choosing the FFT (Fast Fourier Transform) Bandpass filter, ImageJ allows to filter larger structures down to - , and smaller structures up to a certain value of pixels. The software also suppresses vertical or horizontal stripes. In order to find appropriate filter values, different values were tested, as seen in figure 41. The best values were found by filtering larger structures

down to 70-100 pixels and smaller structures up to 1-3 pixels. The choice of pixel value would depend on the magnification of the image, which in this study of cells can vary from ×5 000 to ×8 000. In figure 42 also the vertical stripes from the ion beam are suppressed as described in section 2.4.
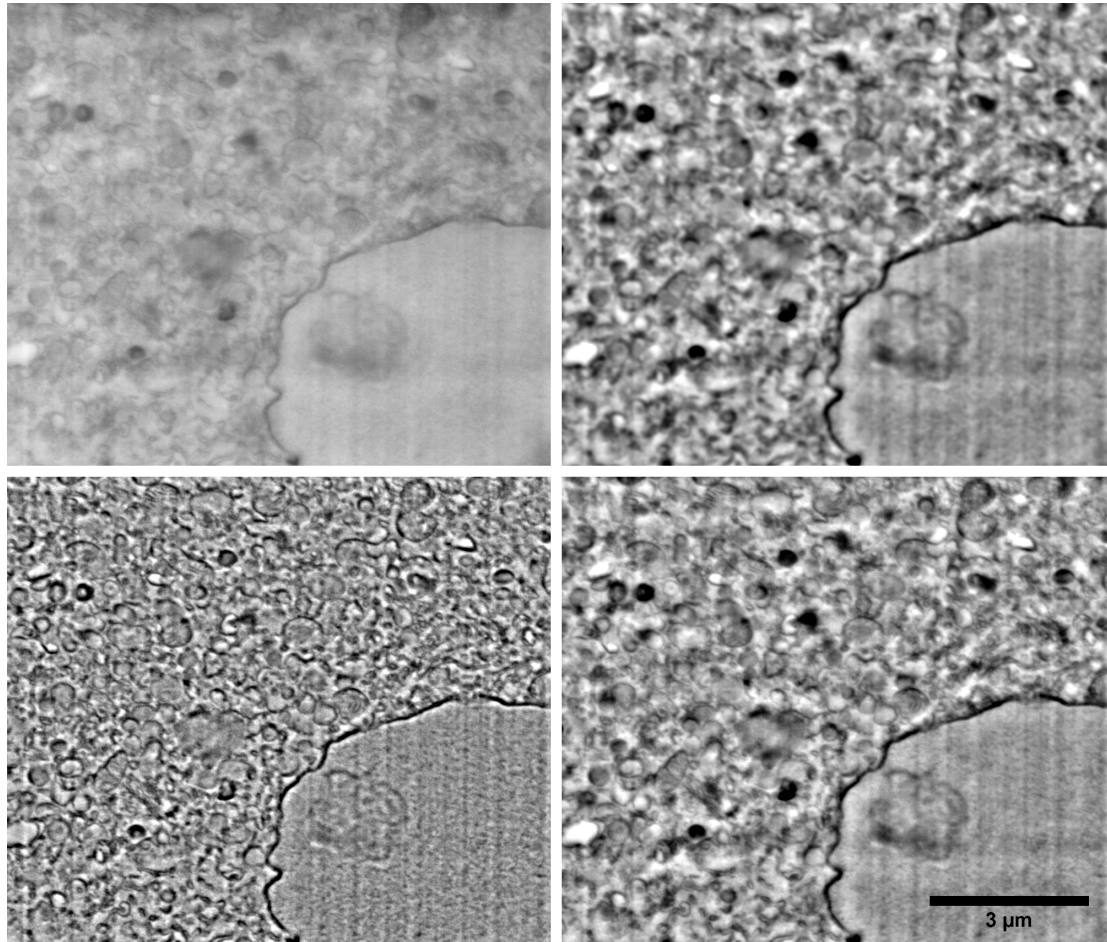
Figure 41: SEM images of the interior of a cell showing ultrastructural features like membranes and vesicles. The upper left image has not been processed in any way, except inverted. The upper right image has been FT processed where smaller structures are filtered up to 10 pixels. This causes the details to blur. The lower left has the larger structures filtered down to 30 pixels which does not improve the signal-to-noise ratio appreciatively and obscures the details. However, the lower right has the the larger structures filtered down to 100 pixels and smaller structures filtered up to 3 pixels. This seems to give an image of better quality in regards of differing the smaller ultrastructural cell details. The images have a magnification of ×8 000.

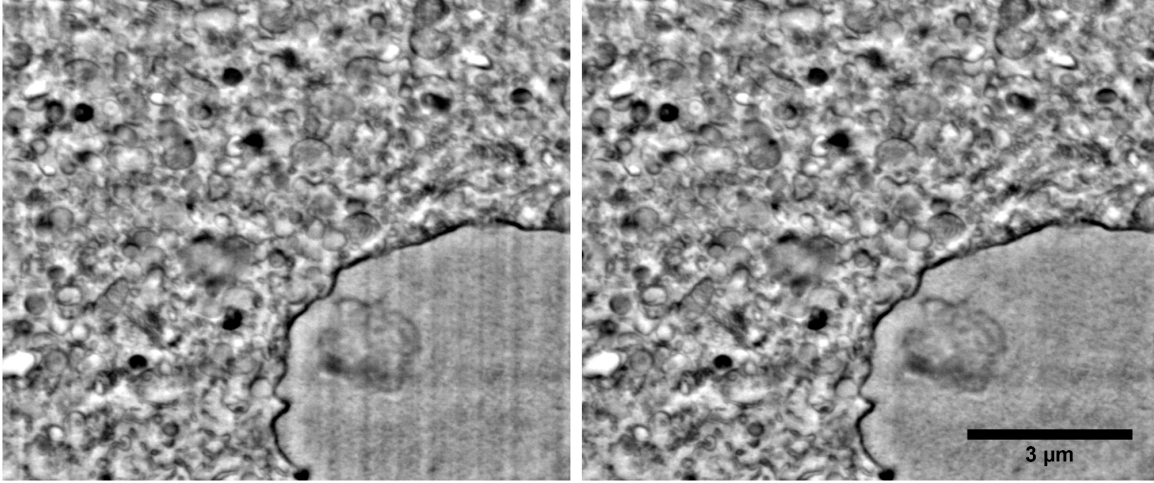**Figure 42:** SEM images of the interior of a cell, where both have been processed with Fast Fourier Transform, but the image to the right have suppressed the vertical lines. The vertical lines are present in the figure to the left and are due to the milling effects of the ion beam. The suppression of the vertical stripes is optional in the ImageJ software. Details on how suppression of stripes works can be found on under section 2.4.

4.2.6 Image correction

Since the images are acquired at an 52 $^\circ$ angle, the structures that are seen, do not have their true shape. Instead, the image will seem a bit 'packed' together in the y-direction. So before any 3D reconstruction can be done, all the images should be resized to the their true size. In figure 43 the geometric setup is illustrated to the left. The right shows how much an 1 μm$\times$1 μm area is resized to the true dimensions; 1 μm$\times$1.27 μm. The correct values are calculated from the geometric setup in figure 43 and using simple trigonometry in eq. 4 and getting the relation between Δy_e, which is the pixel shift on the collected image, and Δy_{true}, which is the shift on the sample, in eq. 5.

$$\sin 52° = \frac{\Delta y_e}{\Delta y_{true}} \tag{4}$$

$$\Delta y_{true} = 1.27 \Delta y_e \tag{5}$$
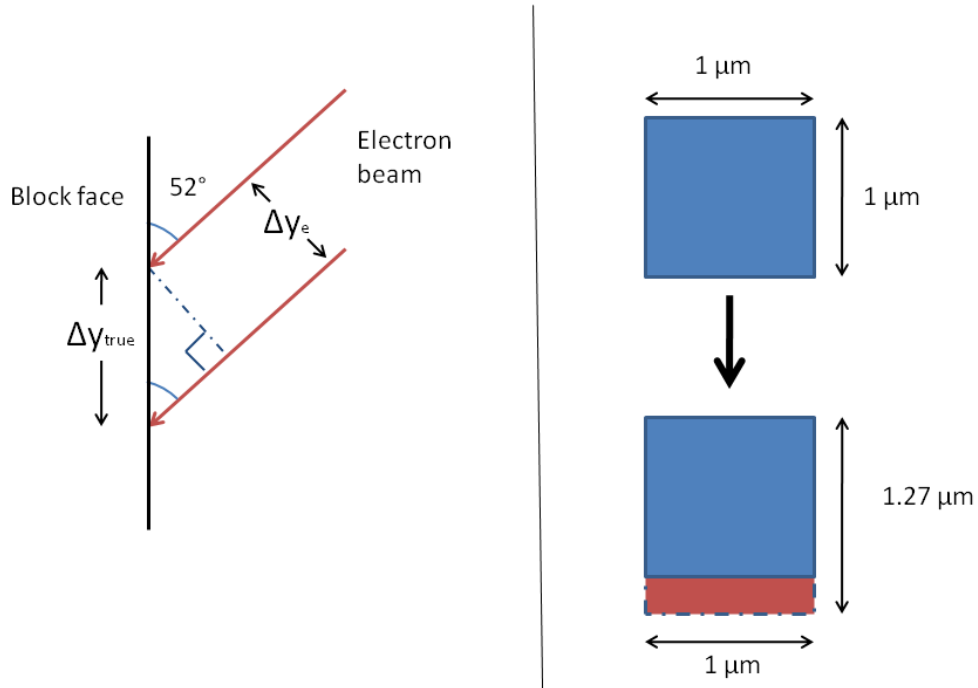
Figure 43: *Left:* Illustration of the geometric setup showing the angle of the electron beam to the block face, where Δy_e (pixel shift on the collected image) corresponds to Δy_{true} (pixel shift on the sample). *Right:* Schematic of an area of 1 μm $\times$ 1μm resized to 1 μm $\times$ 1.27 μm.

Resizing an image can be done using a ImageJ plugin called *Resize*, which allows to change the pixel value in both x- and y-directions [42]. To get the true size from an original acquired image the pixels in the y-direction is increased with a factor of 1.27. Such a resize is done in figure 44. After resizing it is observed that oval structures get more of a circular shape, which is expected.
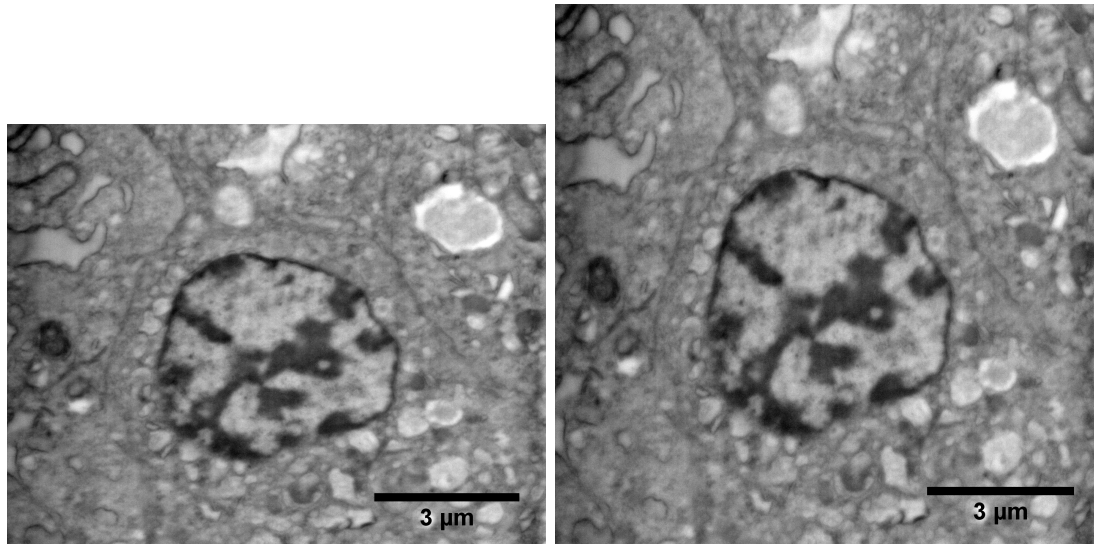
Figure 44: *Left:* An original SEM image of cell structures, including the cell nuclei. *Right:*The same image as to the left, but resized, where the amount of pixels in the y-direction is increased by 1.27 to get the true dimensions of the structures.

Other corrections that need to be accounted for before embarking on the 3D reconstruction, are cell shrinkage/swelling during sample preparation and slice correction. Correcting for the slice thickness, and thus correcting for the resolution in the z-direction, is a matter of instrument calibration. However, this is not been taken to consideration in this project.

Figure 45 shows a montage of 24 serial sectioned images of a macrophage where angle correction and FFT filtering have been done. The montage is part of a larger image stack of 96 slices (see complementary video: Macrophage1.avi).
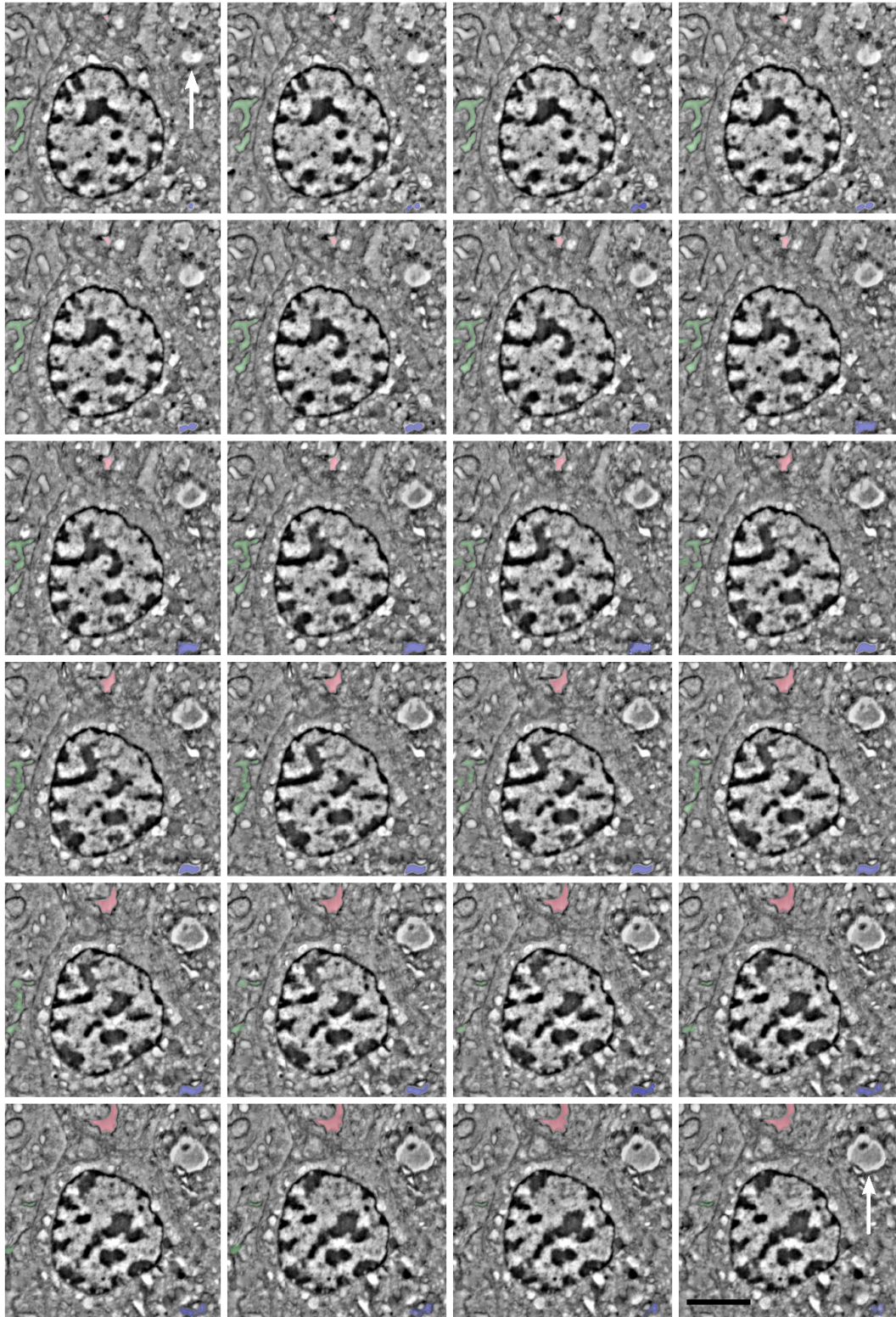
Figure 45: A montage of 24 SEM images sampled from a image stack acquired with slice-and-view showing cross-sections of macrophage from mouse cell features including the cell nuclei. Some features are coloured (green, red and blue) intended to make it easier to follow the changes through the montage. The white arrow points to a feature in the first and last image, that increases in size. The distance between each slice was set to 30 nm, making an estimated total volume of the montage (10.71 μm × 9.48 μm × 0.72 μm) 73.10 μm^3. The scale bar is 1.5 μm. All the images have been FTT filtered and resized. The montage is a part of a larger image stack (see complementary video clip: *Macrophage1.avi*)

4.2.7 Identifying cellular features

TEM is one of the traditional characterization techniques in biotechnology. There exists a lot of knowledge in how tissue should respond to an electron beam and appear in an image. Since the preparation techniques are very similar to what is done for TEM, it is sensible to use TEM data to support whatever findings done with the FIB-SEM. In figure 46 there are two TEM images (top) and two SEM images (bottom)of the the same type of cells (macrophages from mouse). The images have similar features, however, it is evident that TEM provides superior resolution compared to SEM, as the TEM images overall are much more detailed. Nevertheless, keeping in mind that a major goal with this work is to identify cellular structures, which is resolved enough to be able to reconstruct it in 3D, the features in the SEM images are of good enough quality to do so.
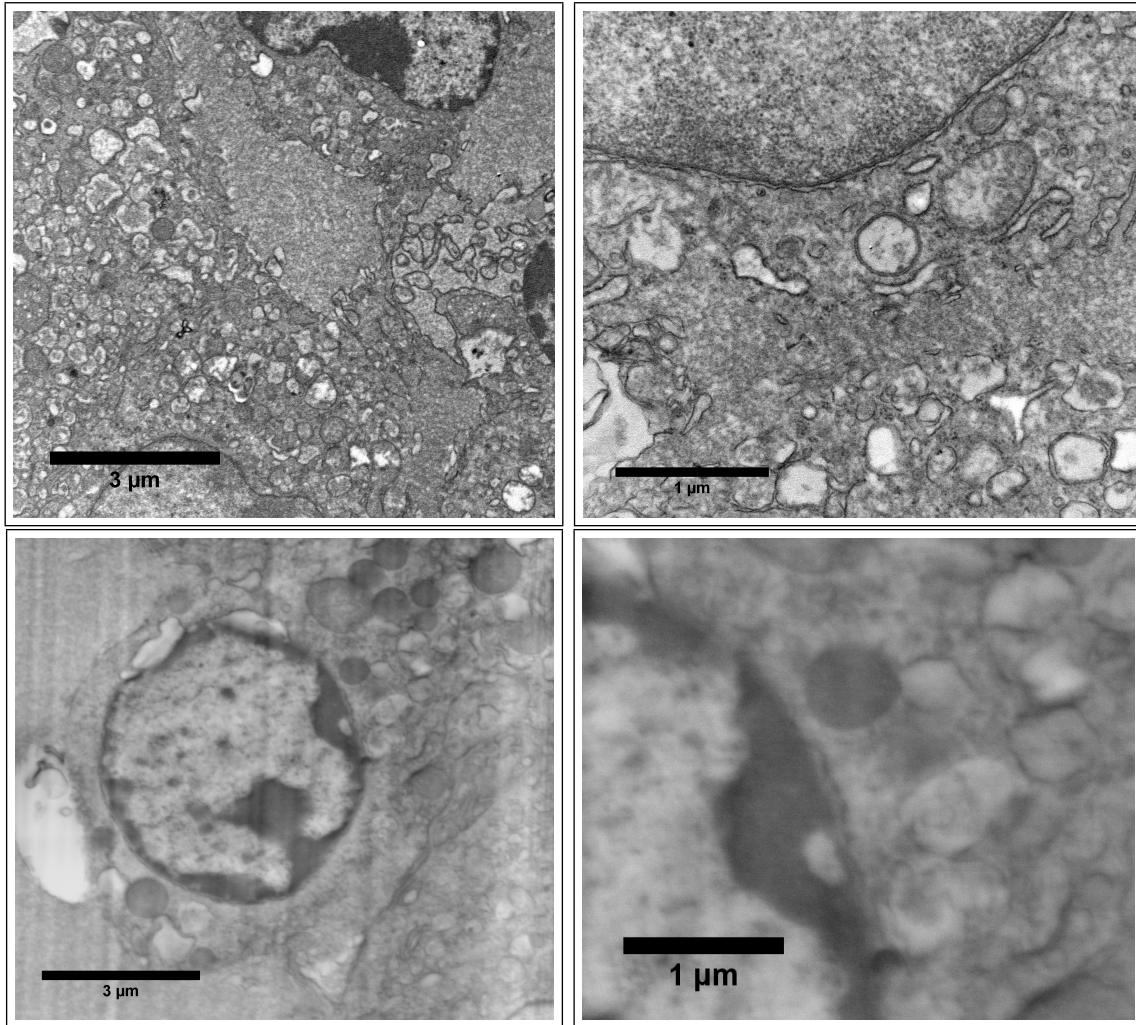
Figure 46: *Top left and top right:* TEM images of macrophages from mouse (courtesy of engineer Nan E. Tostrup Skogaker from Department of Laboratory Medicine, Children's and Women's Health, NTNU). *Lower left and lower Right:* SEM images of macrophages from mouse.

Identifying every detail of a cell in an EM image is a comprehensive task, even for TEM images. However, comparing to what is already identified in the literature [43], there are several cellular features that have characteristic shapes and are fairly easy to recognize, like the *nucleus* and parts of the *golgi apparatus* seen in the left image in figure 48. Studying the image stacks of the macrophages, clearly there are thousands of vesicles which mostly have a constant spherical shape only varying in size and greyscale (contrast differences), as seen in attached video clip *Macrophage2.avi.* The vesicles marked in figure 47 and 48 are thought to be *lysosomes* (**2.**) and a *multivesicular body* (**7.**)(a membrane embedded vesicle containing several other vesicles inside). Also, features that is thought to be *dilated cisternae of granular endoplasmic reticulum* (**6.**) are marked in the right image in figure 48. Vacuoles (**1.**) and mitochondria (**3.**) are also identified in figure 47.
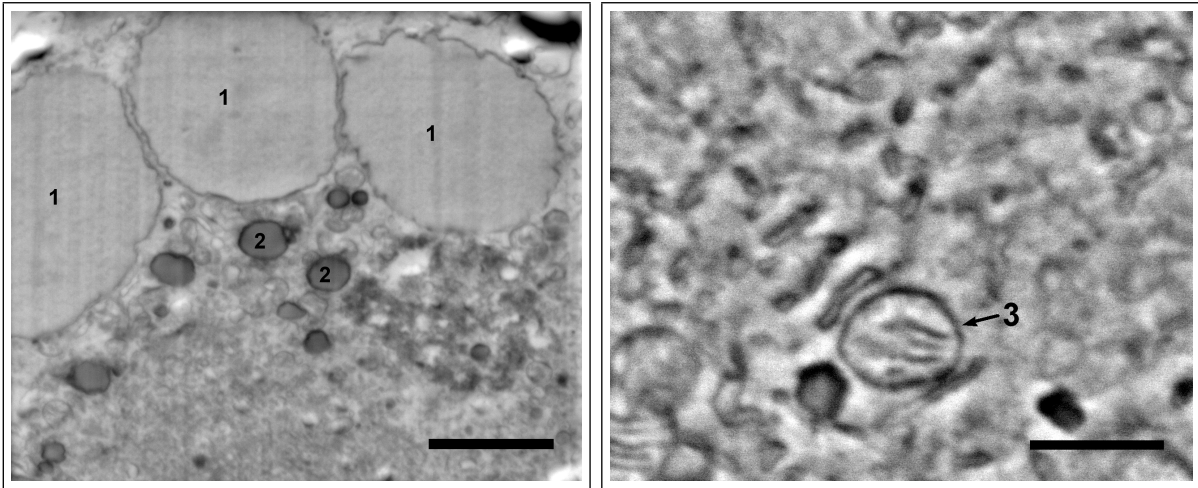
Figure 47: *Left:* **1.** Vacuoles **2.** Lysosomes. The image has a magnification of 6 500× and the scale bar is 4 μm. *Right:* **3.** Mitochondria. The image has a magnification of 25 000× and the scale bar is 750 nm.
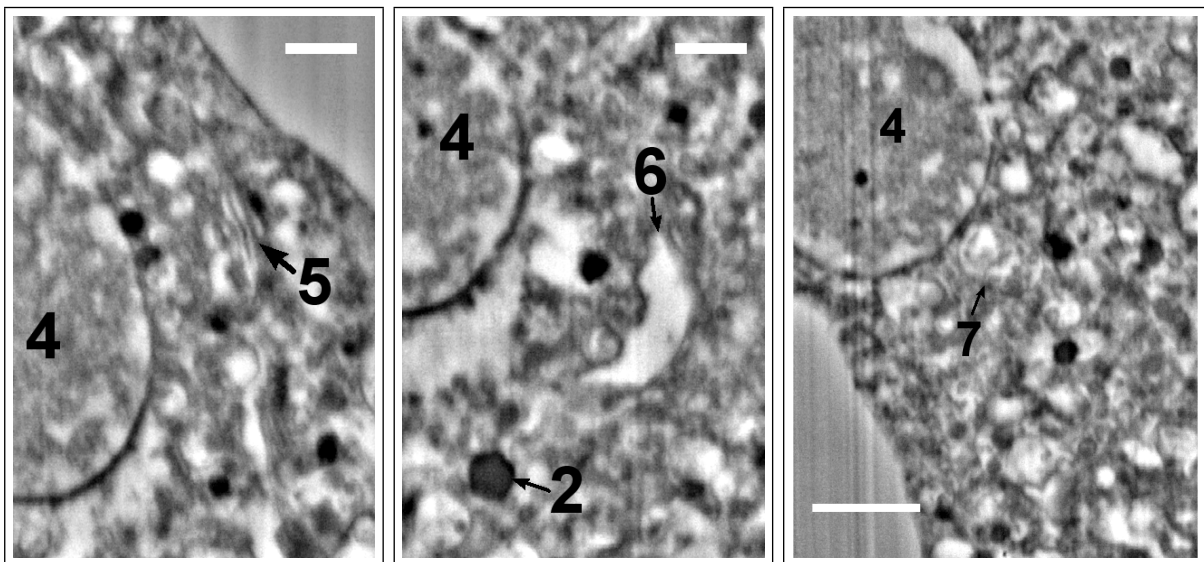
Figure 48: The images have a magnification of 5 000×. *Left:* **4.** Nucleus **5.** Golgi apparatus zone. The scale bar is 1 μm. *Middle:* **6.** Dilated cisternae granular endoplasmic reticulum. The scale bar is 1 μm. *Right:* **7.** Multivesicular body. The scale bar is 2 μm.

4.2.8 3D reconstruction

The following 3D reconstructions are made with ©Imaris Bitplane Scientific Software (usually used for confocal microscopy data) courtesy of Øyvind Halaas, Department for Cancer Research and Molecular Medicine at NTNU. Figure 49, 50 and 51 are made from the complete data set from which the video clip *Macrophage1.avi* is part of.

The software is able to make all organelle surfaces into objects, as seen in figure 49, and thus analyse them based on the original image stack. This makes it also possible to distinguish them by giving the objects different colors (see figure 50), and allows to observe their interaction *e.g.* looking inside them. Imaris has also the ability to link to Matlab, and can then calculate parameters like distances, sizes of organelles, number of interacting specified objects etc.
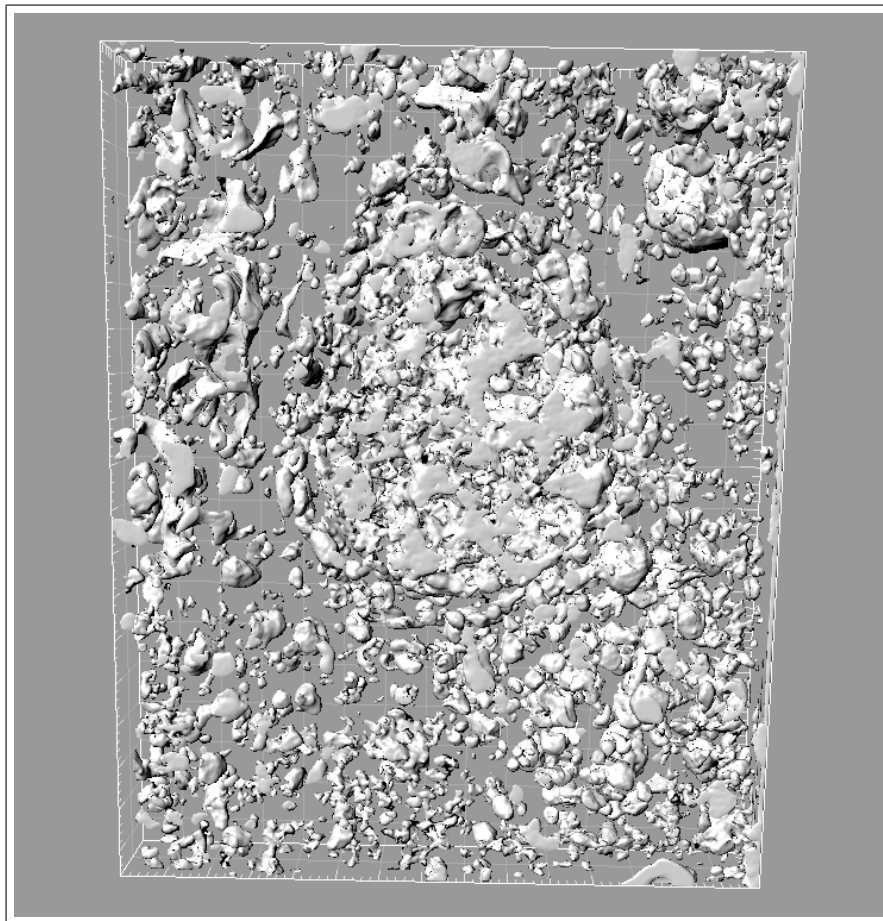
Figure 49: A 3D reconstruction of the same data set from which figure 45 is a part of, using ©Imaris Bitplane Scientific Software (courtesy of Øyvind Halaas, Department for Cancer Research and Molecular Medicine at NTNU).
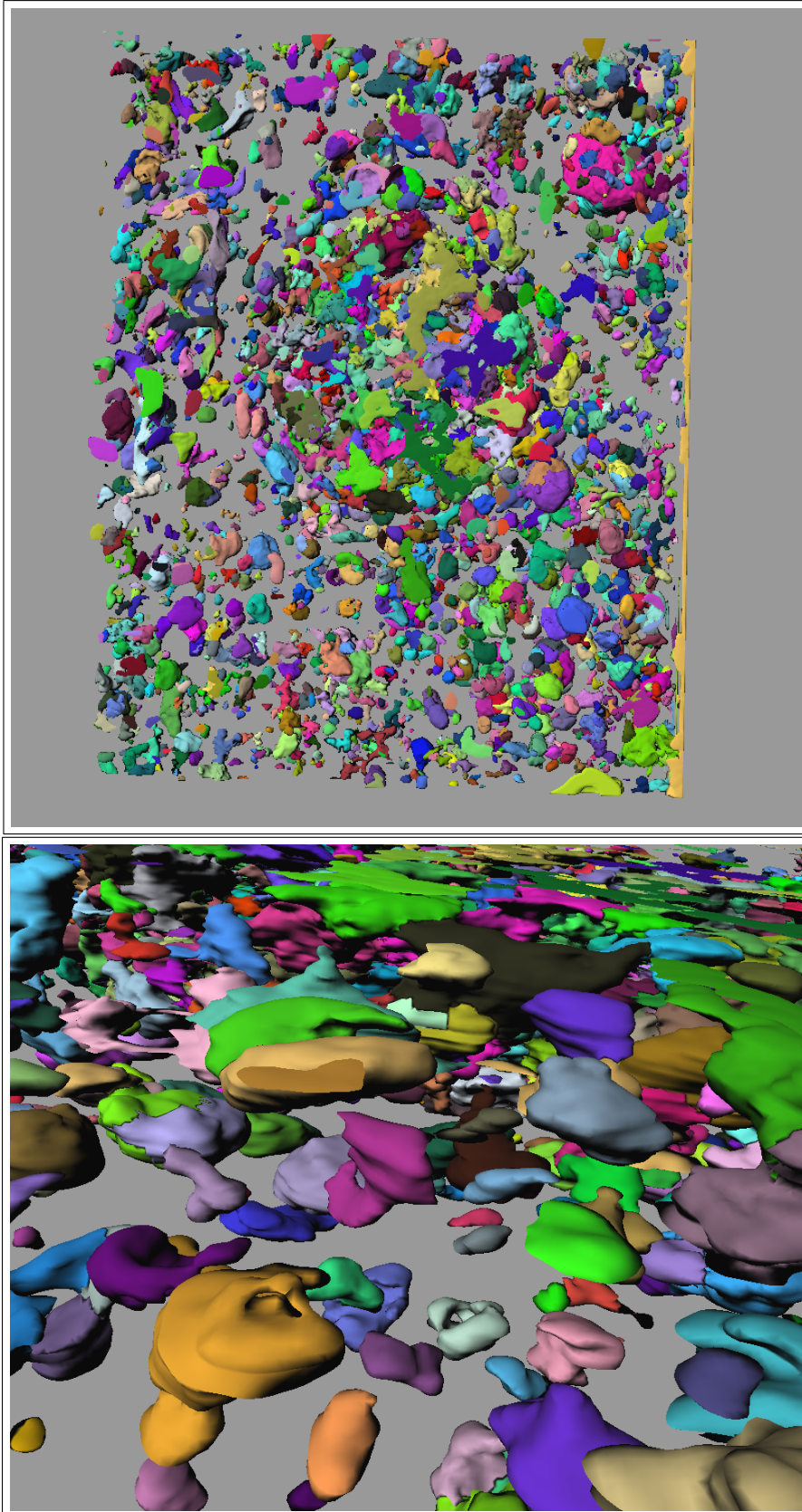
Figure 50: *Top:* A 3D reconstruction of the same image as in figure 49. Here the objects are assigned different colors to be easier distinguished. *Bottom:* A close up of the top image where each object represents an organelle. (Courtesy of Øyvind Halaas, Department for Cancer Research and Molecular Medicine at NTNU.)
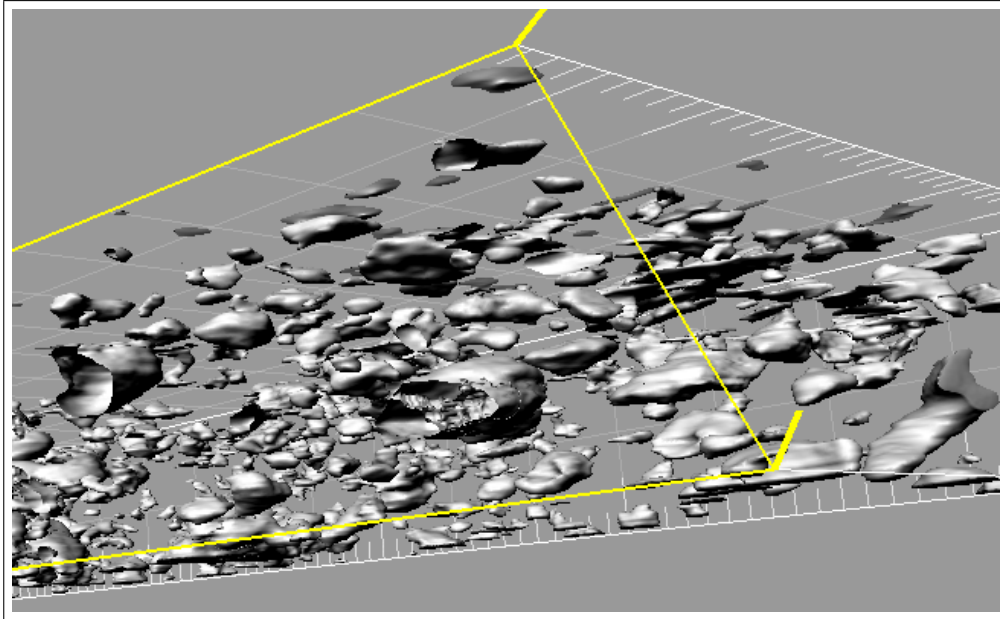
Figure 51: The ©Imaris Bitplane Scientific Software allows to make intersections of the objects to be able to look inside them (courtesy of Øyvind Halaas, Department for Cancer Research and Molecular Medicine at NTNU).

The following figures 52, 53 and 54 are 3D reconstructions from the video clip *Bacteria.avi* (See supporting information). In the top image in figure 52 the whole image stack can be seen as the opacity and threshold has been adjusted. It gives an impression of the whole stack volume. In the bottom image the software has reconstructed surfaces of the cell membrane and other cellular features inside. The software allows to choose a feature of interest and study how it spatially unfolds from all angles as seen in figure 53 and 54. However, it is important to recognize these 3D images as preliminary as more image processing and data collection optimization is needed to give meaningful and interesting data.
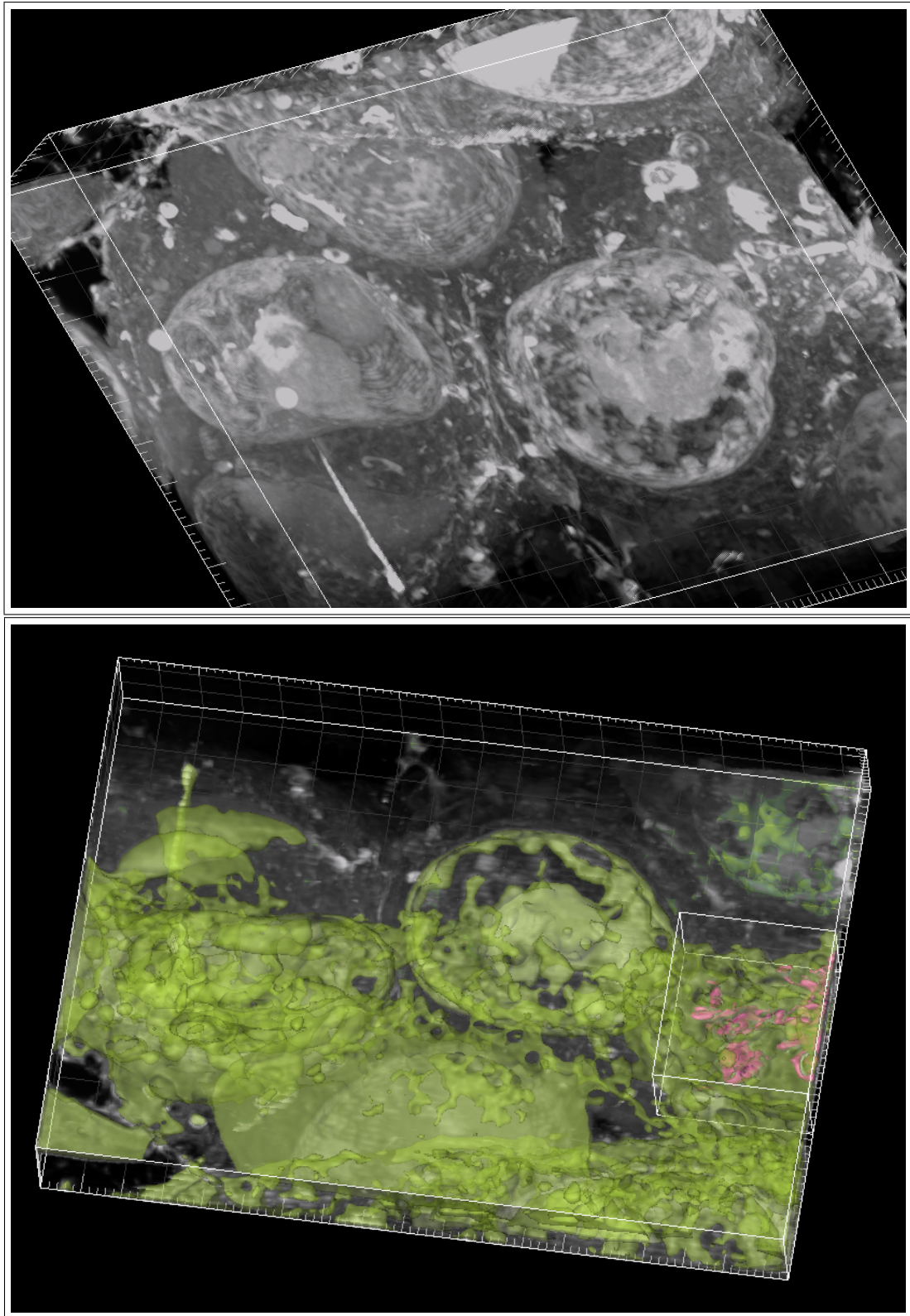
Figure 52: The upper image shows the image stack of *Bacteria.avi*. The threshold and opacity has been adjusted to make the stack transparent enough to visualize the whole stack. In the lower image the software has created a reconstruction of the cell membranes and other cellular features (green), overlapping the original image stack. Interesting features, in this case bacteria, are marked with another color (red). (Courtesy of Øyvind Halaas, Department for Cancer Research and Molecular Medicine at NTNU).
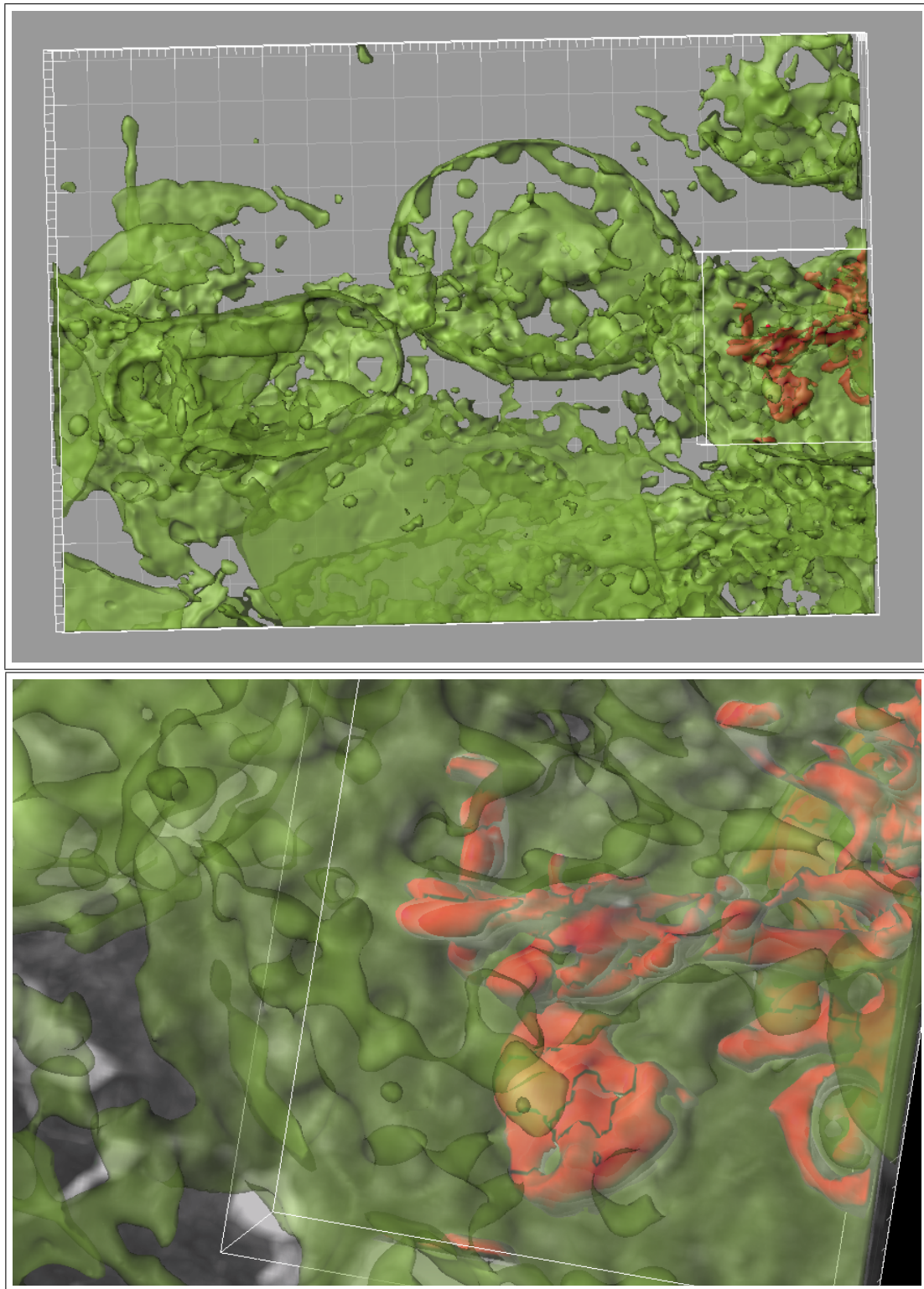
Figure 53: The upper image shows only the reconstruction of figure 52. The lower image is zoomed in on the reconstructed bacteria (red) (Courtesy of Øyvind Halaas, Department for Cancer Research and Molecular Medicine at NTNU).
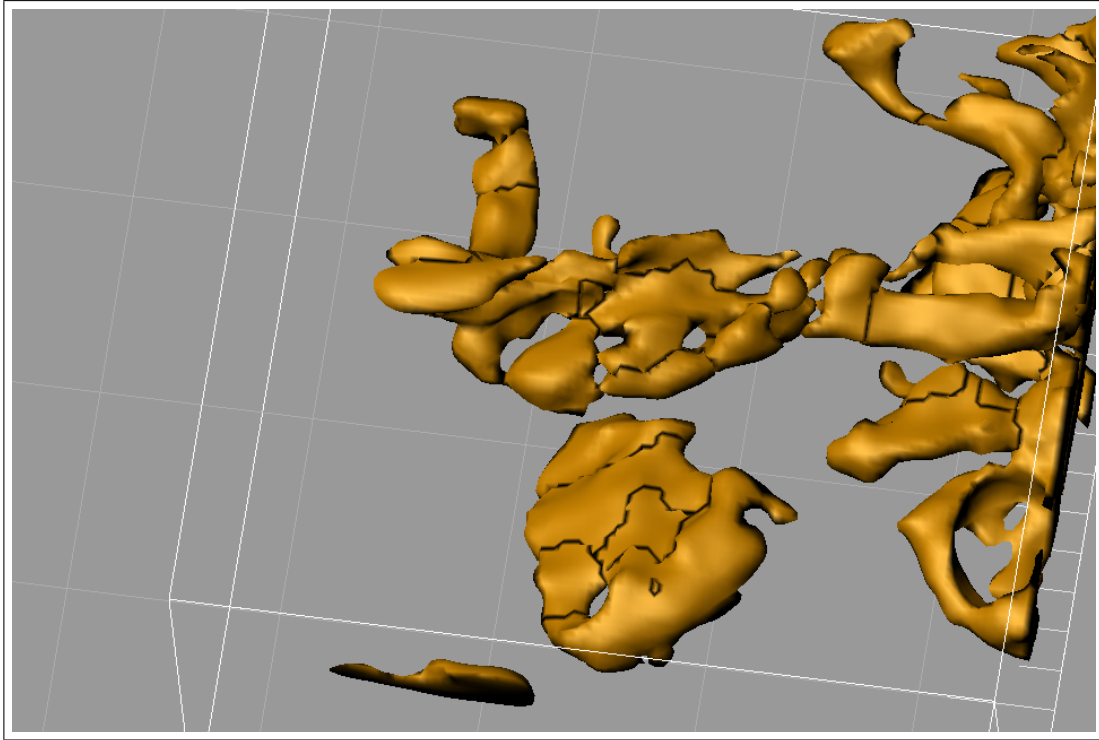
Figure 54: The image is showing the reconstructed bacteria (yellow) alone, from figure 53 (Courtesy of Øyvind Halaas, Department for Cancer Research and Molecular Medicine at NTNU).

4.2.9 Further progress

The images of the embedded cells have been brightness/contrast adjusted and FFT filtered to improve the image quality. Despite these improvements, there is still work that needs to be done for the images to be of optimal quality. Knott *et. al* have been able to obtain SEM images of epoxy embedded brain tissue of excellent quality (see figure 2) compared to the images in this study. Thus proving that there is a potential of improving the characterization approach.

It is reasonable to believe that charging is present in the sample. At high acceleration voltages (10 kV) charging appeared frequently. Although the charging did not manifest itself clearly at 5 kV, it is thought that charging still contributes to worsen the image quality. The embedding material, epoxy resin, is itself not conducting and would readily build up a charge. As mentioned earlier, the preparation in this study is adopted from TEM preparation protocols where charging is not an issue when imaging, due to thin slices, and hence, not taken into consideration. However, the cells are stained with OsO_4 containing electrical conducting osmium and will contribute to a reduction of a local charge [44]. But to ensure that the charging is reduced to a minimum it may

be an option to use electrically conductive epoxy *e.g.* silver-filled epoxy [41]. Silver itself would certainly give a strong signal in SEM as it is has a high atomic number compared to carbon-based tissue, and is likely to disturb the contrast signal from cellular ultrastructures. Nevertheless, sample preparation is an area within this characterization technique that needs more attention.

Looking further on sample preparation, but in terms of staining to enhance contrast of specific parts of a cells, it is unexplored for the use of FIB-SEM. However, staining procedures for TEM-samples is well established, and as there is a somewhat correlation of the contrast from TEM and SEM. The existing knowledge would be of great support when developing customized procedures for FIB-SEM.

Macrophages infested with *mycobacterium avium* are studied as a part of a development of designing a vaccine for tuberculosis[m]. Although not the main focus of this project, interestingly, cytosolic bacterial localization and replication are pathogenic features of mycobacteria that may reveal mechanisms that needs to be understood in order to make a successful vaccine [45]. By using a new staining approach, as described in section 3.1.3, the bacteria where clearly observed with FIB-SEM as seen in figure 55. In these images the bacteria are observed close to vacuoles, as it is thought that the bacteria feed off them. The staining procedure was based on [46, 47, 48] and [49] and is still not perfected for FIB-SEM. A stack was collected of this sample (See supporting information: *Bacteria.avi*).
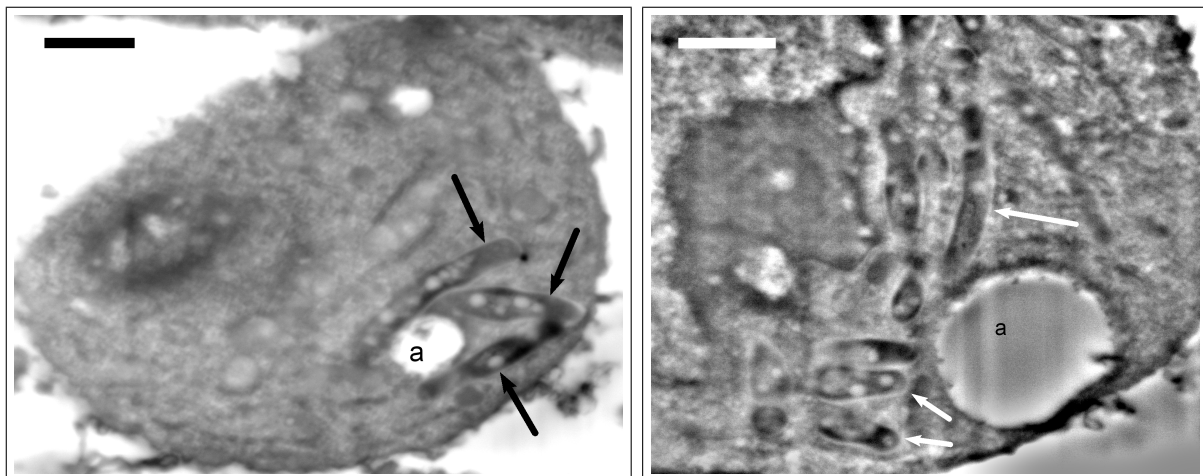
Figure 55: Macrophages infested with mycobacterium avium. Arrows point out where the bacteria are. The bacteria are gathered around vacuoles (**a**) as it is thought that they feed of them. The magnification is ×15 000 (left) and ×20 000 (right) and the scale bar is 1 μm.

---

[m]Tuberculosis kills 50% of its victims. It is estimated that one third of the world's population is infected with tuberculosis.

4.3 Limitations

A major limitation of the FIB-SEM, other than a limit of resolution (compared to TEM), is its destructive nature. Serial sectioning (slice-and-view) mills away the material, not making it possible to go back and collect data if that should be necessary. This would expect the user to have sufficient instrument experience to apprehend accurate data and avoid mishaps. However, it is also worth recognizing that this is still a young technique as the use of FIB-SEM for biological samples can first be seen in 2006 [40]. There is no established approach when it comes to characterizing alginate beads or cells embedded in epoxy with FIB-SEM.

In the case of the epoxy embedded cells, there is an opportunity to collect an image stack of a complete cell (all organelles within the cell membrane). The challenge is to localize where a cell begins, as it is not possible to retrieve data inside the epoxy block. At the time being, the approach would be to choose a volume of interest (VOI) big enough to increase the chance of collecting a stack containing a complete cell.

4.4 Guidelines on how to use FIB on biological samples and biomaterials at NTNU NanoLab

4.4.1 Protocol for acquiring 3D data of mineralized alginate beads

- Use 9 mm carbon tape on a FIB stab and carefully sprinkle the beads on top. Make sure the beads stick by holding the stab upside down and tapping it with your finger.

- Sputter coat the sample with Pt/Pd; first with 20 nm at an angle ($\sim 45\,°$) in rotating mode. Next coat another layer of 20 nm Pt/Pd perpendicularly (no angle). Two layers are necassary to ensure proper contact with the carbon tape to decrease charging effects. Optional: To minimize drifting effects let the carbon tape settle for 24 hours.

- When mounted inside the chamber, use 5 kV as acceleration voltage and 21 pA when looking and navigating the beads with SEM. When looking with the ion beam, use 30 kV and 9.7 pA.

- For rough cutting a U-trench (see figure 15) with the ion beam it is ok to use 6.5 nA at 30 kV as long as the dimensions of the trench is big enough; 10 - 15 μm wide and high. Keep a 10 μm clearance from edge to edge. Set z-size to 1 μm

- Deposit 1 μm (z-size=1μm) platinum on ROI. Use a current of 0.46 nA and acceleration voltage of 30 kV.

Slice and View (FEI Slice & View G2)

- Before beginning slice and view, it is very important to be accurate about the eucentric height. Since the beads are spherical this may be a challenge as the eucentric height will change as you move around on the bead. Verify that the sample is in eucentric height right before slice and view is run.

- Also very important to make sure that fiducial mark is well defined and in focus with the ion beam as the software uses this mark to correct for drift and keep sample stable. However, the sample will always suffer from some drift when acquiring image stacks. It may help to choose a higher resolution for the ion beam, like 1024×884.

- For the electron image choose resolution 2048×1768 and a dwell time of 30 μs.

- Set z-size to 1 μm

- Mill with 2.8 nA at 30 kV (milling data with other currents and acceleration voltages are incomplete).

- Remember to take a picture before (or after) slice & view is run, as the scale bar disappears. This is to set the scale later on. Make sure that the scale-bar picture has the same resolution (same amount of pixels) as the acquired stack.

4.4.2 Protocol for acquiring 3D data from epoxy embedded cells

- Stick the block on a FIB stab using 9 mm carbon tape. Make sure the block is smoothly cut/moulded so there is proper adhesion to the carbon tape.

- Sputter coat the block with Pt/Pd; first with 20 nm at an angle (ca. 45 °). Make sure that the cutting face is upside (gets coated). Next, coat another 20 nm Pt/Pd perpendicularly (no angle). Two layers are necessary to ensure proper contact with carbon tape to decrease charging.

- When the block is mounted inside the chamber, use 5 kV and 2.7 nA when looking and navigating. The ion beam should be set to 30 kV and 9.7 pA, although the block can withstand a higher ion beam current.

- Expose the cells by cutting a thin slice off the block face (see figure 16) with a high ion beam current.

- Find the desired region of interest (ROI).

- Deposit Pt ($z = 0.75 \mu$m) on the top surface using the ion beam at 30 kV and 0.92 nA.

Slice and View (FEI Slice & View G2)

- Find eucentric height.

- Let the fiducial mark be well defined and in focus as the software uses this mark to correct for drift and cut in designated stack. It may help to choose a higher resolution for the ion beam like 1024×884 and adjust contrast/brightness.

- Choose resolution 2048×1768 and dwell time 60 or 100 μs for the electron beam.

- The slice thickness should be 50 nm or below.

- The appropriate magnification depends on the size of area which will collected. A typical magnification is × 6500.

- Images should be acquired at 5 kV and 2.7 nA.

- Use 0.92 nA and 30 kV for the ion beam. Lower currents can be used to decrease the curtaining effect.

- Remember to take a picture before slice & view is run, as the scale bar disappears. This is to set the scale later on. Make sure that the scale-bar picture has the same resolution (same amount of pixels) as the acquired stack.

5 Conclusion

The FIBs ability to mill away material with nanometer precision, implies a great potential when it comes to characterizing biological samples. A major advantage that FIB introduces is the speed and ease of collecting 3D data of high resolution.

The aim of this study was to investigate the possibilities that FIB-SEM can provide for studying the three dimensional structure of biological samples. This would involve gaining initial competence of the technical aspects of the FIB-SEM and sample requirements. As a result, this project presents three main stages in producing a complete 3 dimensional representation; 1) Sample preparation, 2) FIB-SEM serial sectioning and imaging and 3) image processing.

Two different samples were studied; critical point dried mineralized hydrogel alginate beads and cells embedded in epoxy. In the case of the alginate beads, a U-trench needed to be sputtered away. In this way a region of interest is left standing and exposing a cross-section area immediate below the surface (see figure 24). This would allow to do a slice-and-view and successfully collect a 3D data set.

The FIB cell sample preparation was adopted from what is done for TEM-preparation, using the same preparation protocols, and embedding the cells in epoxy. Differing from a TEM-sample, the FIB demands a bulk sample that makes it possible to serially cut sections off it. Different shapes of the hardened epoxy resin were tried to find the best geometry for serial sectioning. The block geometry proved to meet the requirements for achieving serial cuts of even and smooth slices.

Finding the appropriate parameters for sectioning, heavily depends on what material the specimen is made of and what dimensions of interest are. The porous mineralized alginate hydrogel beads showed various degrees of stability as sufficient milled trenches were heavily dependent on the dimensions of the trench and the ion beam current. Also, the spherical shape of the beads is not accounted for in the slice&view-software. Additionally, the high porosity and structural instability could also cause severe drifting during image collection. Despite these challenges, high resolution from the interior architecture was acquired. Opposed to the beads, cells embedded in epoxy resin is a hard and stable material (epoxy is a heavily cross linked polymer [41]) and is therefore easier to work with as it responds to the ion beam (milling) in a more predictable fashion, and much less drift is observed.

Acquiring images for the two materials, rely on two different contrast mechanisms. The porosity of the bead would give excellent topographic contrast from secondary electrons, and high resolution could be achieved. Features of 10 nm could be observed. For the

69

epoxy embedded cells the cross-sections are completely flat, thus relying on compositional contrast. Staining the cellular membranes with uranyl acetate and OsO_4, ultrastructural features with high resolution could be seen (*e.g.* cristae in mitochondria).

Different detector modes were tested to find the optimal image quality. It is interesting that also the compositional contrast was observed with secondary electrons, when conventionally backscattered electrons would be used. However, it is thought that the difference between the atomic number in the stain and in the surrounding material, was large enough that also SE would give a difference in signal. The images were collected using the Everhart-Thornley detector (ETD).

Also, experimenting with different voltages, to collect images of the best quality, was done. 5 kV proved to be the better option as 2 kV and 10 kV was also tested.

An alternative staining procedure was also tried with the intention to get better contrast from *mycobacteria avium*. The study of this bacteria is in the context of finding a vaccine for tuberculosis. In this procedure, the cells were also stained with *rutenium red* which would enhance the contrast of the bacteria. The bacteria were easily localized, thus implying a versatility of the technique in terms of specificity. In other words, the possibility of developing procedures for achieving specific goals depending on what the medical question is.

For this study, image processing mainly includes correcting for drift (alignment), FFT filtering (to increase the signal-to-noise ratio and and suppressing vertical lines) and correcting for the viewing angle. When this is done the image data set was ready to be reconstructed in 3D. However, the reconstruction done in this study is very preliminary as more image processing is needed.

From the experience gained during instrument time, instructional guidelines of how to operate the FIB-SEM has been developed. The guide contains steps on how get the finished prepared sample ready for the FIB-SEM, and appropriate parameters for setting up the slice & view software.

CLSM has traditionally been an easy-to-use technique to get good images of biological material in three dimensions. This project proves that it is now possible to obtain 3D data sets of much better quality. SEM has always been superior in resolution compared to CLSM, and when combined with a FIB, collecting image stacks has become a relatively easy task. The goal that developed during the project, was not to obtain the same resolution as TEM, but a resolution sufficient enough to clearly resolve the biopolymer structure and cellular features. It is demonstrated that FIB-SEM do fulfill these criteria, but still have potential to be improved at all stages.

The importance of retrieving 3D data from biological tissue in a relatively fast and easy manner, can prove to heavily inflict the field of characterization and change the way researchers would approach medical questions as FIB-SEM represents a new generation of characterization tools. If this trend continues, FIB-SEM will be a technique routinely applicable to biological samples.

References

[1] K. R. Ervik, "Characterizing alginate beads with confocal laser scanning microscopy, scanning electron microscopy and focused ion beam," 2010.

[2] R. Hermann, P. Walther, and M. Mller, "Immunogold labeling in scanning electron microscopy," *Histochemistry and Cell Biology*, vol. 106, pp. 31–39, 1996. 10.1007/BF02473200.

[3] J. Zhou, C. Leuschner, C. Kumar, J. Hormes, and W. Soboyejo, "A tem study of functionalized magnetic nanoparticles targeting breast cancer cells," *Materials Science and Engineering: C*, vol. 26, no. 8, pp. 1451 – 1455, 2006. Proceedings of the First TMS Symposium on Biological Materials Science.

[4] J. Hecksher-Srensen and J. Sharpe, "3d confocal reconstruction of gene expression in mouse," *Mechanisms of Development*, vol. 100, no. 1, pp. 59 – 63, 2001.

[5] M. Born and E. Wolf, *Principles of Optics*. Cambridge University Press, 1997.

[6] W. H. Massover, "New and unconventional approaches for advancing resolution in biological transmission electron microscopy by improving macromolecular specimen preparation and preservation," *Micron*, vol. 42, no. 2, pp. 141 – 151, 2011. Biological Specimen Preparation and Preservation for High Resolution Microscopies.

[7] R. M. K. C. D. Erni, Rolf, "Atomic-resolution imaging with a sub-50-pm electron probe," *Physical Review Letters*, vol. 102 (9): 096101, 2009.

[8] A. Merchan-Perez, J.-R. Rodriguez, L. AlonsoNanclares, A. Schertel, and J. DeFelipe, "Counting synapses using fib/sem microscopy: a true revolution for ultrastructural volume reconstruction," *Frontiers in Neuroanatomy*, vol. 3, no. 0, 2009.

[9] P. Hortol, "Sem analysis of red blood cells in aged human bloodstains," *Forensic Science International*, vol. 55, no. 2, pp. 139 – 159, 1992.

[10] S. Rao, K. S. Furukawa, T. Mizumi, T. Ushida, and T. Tateishi, "Sem analysis of primary murine macrophage cells challenged by pe beads, in vitro and in vivo uhmwpe wear debris and evaluation of subsequent release of il-6," *Materials Science and Engineering: C*, vol. 17, no. 1-2, pp. 113 – 117, 2001.

[11] B. D. and K. W. D., *Microstrucural Characterization of Materials*. Wiley, 2008.

[12] J. I. Goldstein, *Scanning Electron Microscopy and X-Ray Mircoanalysis, Second Edition.* Springer, 1992.

[13] T. Ogura, "A high contrast method of unstained biological samples under a thin carbon film by scanning electron microscopy," *Biochemical and Biophysical Research Communications*, vol. 377, no. 1, pp. 79 – 84, 2008.

[14] J. J. Bozzola and L. D. Russel, *Electron Microscope - Principles and Techniques for Biologists , Second Edition.* Jones and Bartlett Publishers, 1992.

[15] N. Yao, *Focused Ion Beam Systems: Basics and Applications.* Cambridge, 2007.

[16] M. U. J. Orloff and L. Swanson, "High resolution focused ion beams; fib and its applications," *New York: Kluwer Academic/Plenum Publishers*, pp. 21–77, 2003.

[17] A. Z. V. L. M. B. Z. D. Drobne, M. Milani, "Electron and ion imaging of gland cells using thefib/sem system," *Journal of Microscopy*, vol. 219, pp. 29+35, 2005.

[18] D. Drobne, M. Milani, V. Leser, F. Tatti, A. Zrimec, N. Znidarsic, R. Kostanjsek, and J. Strus, "Imaging of intracellular spherical lamellar structures and tissue gross morphology by a focused ion beam/scanning electron microscope (fib/sem)," *Ultramicroscopy*, vol. 108, no. 7, pp. 663 – 670, 2008.

[19] S. D. H. L. G. K. e. a. Bennett AE, Narayan K, "Ion-abrasion scanning electron microscopy reveals surface-connected tubular conduits in hiv-infected macrophages," *PLoS Pathog*, vol. 5(9), 2009.

[20] E. Schroeder-Reiter, F. Prez-Willard, U. Zeile, and G. Wanner, "Focused ion beam (fib) combined with high resolution scanning electron microscopy: A promising tool for 3d analysis of chromosome architecture," *Journal of Structural Biology*, vol. 165, no. 2, pp. 97 – 106, 2009.

[21] G. Knott, H. Marchman, D. Wall, and B. Lich, "Serial section scanning electron microscopy of adult brain tissue using focused ion beam milling," *The Journal of Neuroscience*, vol. 28, no. 12, pp. 2959–2964, 2008.

[22] R. L. Felts, K. Narayan, J. D. Estes, D. Shi, C. M. Trubey, J. Fu, L. M. Hartnell, G. T. Ruthel, D. K. Schneider, K. Nagashima, J. W. Bess, S. Bavari, B. C. Lowekamp, D. Bliss, J. D. Lifson, and S. Subramaniam, "3d visualization of hiv transfer at the virological synapse between dendritic cells and t cells," *Proceedings of the National Academy of Sciences*, vol. 107, no. 30, pp. 13336–13341, 2010.

[23] Y.-P. Fang, Y.-B. Huang, P.-C. Wu, and Y.-H. Tsai, "Topical delivery of 5-aminolevulinic acid-encapsulated ethosomes in a hyperproliferative skin animal model using the clsm technique to evaluate the penetration behavior," *European Journal of Pharmaceutics and Biopharmaceutics*, vol. 73, no. 3, pp. 391 – 398, 2009.

[24] R. Hochberg and S. Atherton, "A new species of lepidodasys (gastrotricha, macrodasyida) from panama with a description of its peptidergic nervous system using clsm, anti-fmrfamide and anti-scpb," *Zoologischer Anzeiger - A Journal of Comparative Zoology*, vol. 250, no. 2, pp. 111 – 122, 2011.

[25] B. T. S. Catharina de Lange Davies, *Biophysical Nanotechnologies, Lecture notes TFY 4265, Biophysical Microtechniques.* 2008.

[26] B. B. Mary Bell, *Artifacts in Biological Electron Microscopy.* Plenum Press - New York and London, 1988.

[27] J. Cazau, "About the role of the various types of secondary electrons (se1; se2; se3) on the performance of lvsem," *Journal of Microscopy*, vol. 214, 2004.

[28] E. B. Online, "Fermi level." http://www.britannica.com/EBchecked/topic/204779/Fermi-level. May 2011.

[29] H. Seiler, "Microporous microchannel plates and method of manufacturing same," *J. Appl. Phys.,*, vol. 54, No.11, pp. R1–R18, 1983.

[30] H. Z. Jun Xu, Wenxiong chen, "Composition contrast in high resolution secondary electron image," *Journal of Chinese Electron Microscopy Society*, vol. 16, pp. 1+5, 1997.

[31] P. Li, S. Bao, D. Zhang, L. Zhuang, and L. Ma, "Application of secondary electron composition contrast imaging method in microstructure studies on the microwave tube barium-tungsten cathode," in *Computational Problem-Solving (ICCP), 2010 International Conference on*, pp. 16 –18, dec. 2010.

[32] "Fourier transforms." http://homepages.inf.ed.ac.uk/rbf/HIPR2/fourier.htm, May 2011.

[33] Brayer, "Introduction to fourier transforms for image processing," *http://www.cs.unm.edu/ brayer/vision/fourier.html.*

[34] A. W. R. Fisher, S. Perkins and E. Wolfart., "Fourier transforms." http://homepages.inf.ed.ac.uk/rbf/HIPR2/fourier.htm, 2003. June 2011.

[35] R. Gonzales and R. Woods, *Digital Image Processing.* Addison-Wesley Publishing Company, 1992.

[36] S. S. O. Xie, Andreassen and Sikorski., "Alginate-controlled formation of nanoscale calcium carbonate and hydroxyapatite mineral phase within hydrogel networks," *Acta Biomater*, 2010.

[37] D. M. D. WINTER, C. SCHNEIJDENBERG, M. LEBBINK, B. LICH, A. VERKLEIJ, M. DRURY, and B. HUMBEL, "Tomography of insulating biological and geological materials using focused ion beam (fib) sectioning and low-kv bse imaging," *Journal of Microscopy*, vol. 233, no. 3, pp. 372–383, 2009.

[38] P. Thévenaz, U. Ruttimann, and M. Unser, "A pyramid approach to subpixel registration based on intensity," *IEEE Transactions on Image Processing*, vol. 7, pp. 27–41, January 1998.

[39] "Imagej documentaion wiki, fast fourier transform." http://imagejdocu.tudor.lu/doku.php?id=gui:process:fft, January 2010. March 2011.

[40] P. Schneider, M. Meier, R. Wepf, and R. Mller, "Serial fib/sem imaging for quantitative 3d assessment of the osteocyte lacuno-canalicular network," *Bone*, vol. In Press, Corrected Proof, pp. –, 2011.

[41] C. A. May, *Epoxy Resins: Chemistry and Technology (Second ed.).* New York: Marcel Dekker Inc, 1987.

[42] A. Muñoz Barrutia, T. Blu, and M. Unser, "Least-squares image resizing using finite differences," *IEEE Transactions on Image Processing*, vol. 10, pp. 1365–1378, September 2001.

[43] J. A. Rhodin, *An Atlas of Histology London Toronto.* New York, Oxford University Press, 1975.

[44] V. LEER, D. DROBNE, . PIPAN, M. MILANI, and F. TATTI, "Comparison of different preparation methods of biological samples for fib milling and sem investigation," *Journal of Microscopy*, vol. 233, no. 2, pp. 309–319, 2009.

[45] N. van der Wel, D. Hava, D. Houben, D. Fluitsma, M. van Zon, J. Pierson, M. Brenner, and P. J. Peters, "M. tuberculosis and m. leprae translocate from the phagolysosome to the cytosol in myeloid cells," *Cell*, vol. 129, no. 7, pp. 1287 – 1298, 2007.

[46] T. A. Fassel and C. E. Edmiston, "Ruthenium red and the bacterial glycocaly," *Biotechnic & Histochemistry*, vol. 74, no. 4, pp. 194–212, 1999.

[47] M. Locke and N. Krishnan, "Hot alcoholic phosphotungstic acid and uranyl acetate as routine stains for thick and thin sections," *The Journal of Cell Biology*, vol. 50, pp. 550–557, 1971.

[48] N. K. M. Locke and J. T. McMahon, "M. locke, n. krishnan, and j. t. mcmahon," *Cell Biol.*, vol. 50, pp. 540–544, 1971.

[49] P. K. Rivlin and P. A. Raymond, "Use of osmium tetroxide-potassium ferricyanide in reconstructing cells from serial ultrathin sections," *Journal of Neuroscience Methods*, vol. 20, no. 1, pp. 23 – 33, 1987.

6 Supporting Information

Video clip information

The video clips attached are recommended to be run in VLC media player.

Alginate.avi

Critical point dried mineralized alginate bead

80 sections, 25 nm thick slices

Total volume of 1178 nm×1215 nm×2000 nm

Magnification of 65 000×

Resolution 1024×943

Scale bar 200 nm

12 fps

Macrophage1.avi

Macrophage embedded in epoxy.

96 sections, 30 nm thick slices

Total volume 5.82 μm×7.30 μm×2.88 μm

Magnification of 8 000×

Resolution 2048×1887

Scale bar 1μm

12 fps

Macrophage2.avi

Macrophage embedded in epoxy.

277 sections, 40 nm thick slices

Total volume of 16.92 μm×13.38 μm×11.08 μm

Magnification 5 000×

Resolution 2048×1887

Scale bar 4μm

12 fps

Bacteria.avi

Macrophages infested with mycobacteria avium.

244 sections, 40 nm thick slices

Total volume of 17.61 μm×15.80 μm×9.76 μm

Magnification of 6 500×

Resolution 2048×1887

Scale bar 3μm

12 fps